Quaternary Science Reviews 266 (2021) 107069

Contents lists available at ScienceDirect

Quaternary Science Reviews

journal homepage: www.elsevier.com/locate/quascirev

Sea-ice, primary productivity and ocean temperatures at the Antarctic marginal zone during late Pleistocene

Julian D. Hartman [a], F. Sangiorgi [a, *], M.A. Barcena [b], F. Tateo [c], F. Giglio [d], S. Albertazzi [e], F. Trincardi [e], P.K. Bijl [a], L. Langone [d], A. Asioli [e]

[a] Department of Earth Sciences, Utrecht University, Utrecht, the Netherlands
[b] Departamento de Geologia, Facultad de Ciencias, Universidad de Salamanca, Salamanca, Spain
[c] Istituto di Geoscienze e Georisorse, Consiglio Nazionale delle Ricerche, Padova, Italy
[d] Istituto di Scienze Polari, Consiglio Nazionale delle Ricerche, Bologna, Italy
[e] Istituto Scienze Marine, Consiglio Nazionale delle Ricerche, Bologna, Italy

ARTICLE INFO

Article history:
Received 21 November 2020
Received in revised form
25 June 2021
Accepted 25 June 2021
Available online 15 July 2021

Handling Editor: A. Voelker

Keywords:
Antarctica
Sea ice
Ross sea
Productivity
Water temperature
Pleistocene
Micropaleontology
Organic geochemistry
Element geochemistry
Glacial-interglacial variability
Paleoclimatology

ABSTRACT

While Pleistocene glacial-interglacial cycles are commonly associated with strong waxing and waning of Northern Hemisphere ice sheets, the response of the Antarctic ice sheet and regional changes in oceanographic and environmental conditions to Pleistocene climate dynamics remain poorly constrained. We present a reconstruction of sea-ice cover, sea surface temperature and primary productivity off the Ross Sea margin (Adare Basin at the slope of the Drygalski Basin) during the marine isotope stages (MIS) 9 to 5 (350–70 thousands years ago, encompassing Terminations IV to II). Our multiproxy study relies on micropaleontology (diatoms, dinoflagellate cysts, benthic foraminifers), organic and inorganic geochemistry proxies (carbon and nitrogen isotopes, lipid biomarkers, XRF-data), and sedimentology (IRD) obtained from deep-sea core AS05-10. For each glacial-interglacial transition a clear succession of events can be observed: (near-)permanent sea ice cover during glacial stages is followed by ice-shelf break-up with episodic ice-free areas and surface water stratification. Notably, ice-shelf break-up precedes the increase in air temperature as measured in the Vostok ice core for each glacial-interglacial transition. Generally, air temperature over Vostok starts rising once sea-ice cover at site AS05-10 has significantly decreased, becoming seasonal, as indicated by the diatom species composition. This is also reflected by the high diatom productivity and increased water mixing at site AS05-10, which is indicative of its proximity to the Marginal Ice Zone. At the onset of Termination II (MIS6 to 5), high export productivity and dysoxic bottom water conditions occurred, while water temperature increased about 5 °C. During each interglacial spring/summer sea-ice cover is most reduced, and highest productivity occurs. Following each interglacial, the warm and cold fluctuations match the sawtooth character of the temperatures over Vostok. This record illustrates that at the Ross Sea margin, sea surface conditions and (export) productivity were strongly influenced by the natural climate variability of the Pleistocene. In light of this, current global warming may lead to increased ice-shelf break-up, water column stratification and shifts in the position/size of the Marginal Ice Zone with implications for algal species composition and diversity, and for primary productivity.

1. Introduction

Antarctic sea ice plays a key role in regional polar climate and biology, and global ocean circulation. It forms a regional physical barrier between the atmosphere and the ocean, limiting gas exchange (Stephens and Keeling, 2000), and between warm ocean waters and the ice sheet (Rintoul, 2018). Its reflective surface, which covers 18.2*10^6 km^2 at its maximum extent (1981–2010 monthly mean, National Snow and Ice Data Center), is fundamental for Earth's albedo. In addition, the seasonal melting of sea ice and release of nutrients is responsible for up to 35% of the total primary production (PP) in the Southern Ocean (Garrison and Close, 1993;

* Corresponding author.
E-mail addresses: juulhartman@gmail.com (J.D. Hartman), F.Sangiorgi@uu.nl (F. Sangiorgi).

https://doi.org/10.1016/j.quascirev.2021.107069

Lizotte, 2001). The PP within the sea ice also 'seeds' surface waters upon melting and the entire polar ecosystem depends on the annual cycle of melting and formation of sea ice (Stoecker et al., 2000; Lizotte, 2001; Garrison et al., 2005; Murphy et al., 2017). While, over the last decades, global warming is clearly negatively affecting the sea-ice extent in the Arctic (Comiso and Nishio, 2008; Kay et al., 2011; Notz and Marotzke, 2012), sea-ice extent around Antarctica is more variable and shows strong local differences (Comiso and Nishio, 2008; Turner et al., 2009; Parkinson and Cavalieri, 2012; Parkinson, 2019). The lack of a clear trend in recent times makes future Antarctic sea-ice projections highly uncertain (Arzel et al., 2006; Bracegirdle et al., 2008; Bintanja et al., 2015). In recent years (2016–2017) sea ice has reached a springtime low (Turner et al., 2017), particularly in the Ross Sea sector, that includes the Adare Basin (Parkinson, 2019). Sea ice decline will likely act as a positive feedback to current global warming (e.g., Serreze and Barry, 2011; Park et al., 2015; Abe et al., 2016; Haumann et al., 2016; Andry et al., 2017), which increases the relevance of understanding future sea ice conditions.

The biological response to sea ice decline is difficult to project (Sarmiento et al., 2004). Increased sea ice meltback will promote primary productivity (PP) by increasing available light and nutrient release, so that CO_2 uptake through photosynthesis acts as a negative feedback to global warming (Peck et al., 2010; Fernandez-Mendez et al., 2015). However, with a retreating sea-ice margin, global displacement of high-productivity areas to higher latitudes will reduce their size (Sarmiento et al., 2004). Furthermore, stratification (by melting) and reduced mixing could limit nutrient availability and promote ecosystem changes, which reduces CO_2 drawdown to the ocean floor (Arrigo et al., 1999; Steinacher et al., 2010; Vancoppenolle et al., 2013).

One way to understand the response of PP and sea-ice changes to different climate conditions is to reconstruct these parameters for past warmer than present periods, using sediment records. The Last Interglacial (LIG, 130-116 ka) or Marine Isotope Stage (MIS) 5e is the most recent of these periods. During the LIG, the ocean-area-weighted average sea surface temperature (SSTs) was about 0.7 ± 0.6 °C warmer than preindustrial temperatures (McKay et al., 2011). The LIG may not be the perfect analogue for future climate, because global warmth was induced by Earth's orbital configuration rather than higher atmospheric CO_2 (Petit et al., 1999; Lüthi et al., 2008; Berg et al., 2011). Still, the response of sea-ice concentrations to warmer air and seawater temperatures during the LIG and in a future 2°C-warming scenario is likely very similar because of a (near) equal geographic setting, ice sheet configuration and oceanography. Tracking the summer sea-ice extension and the associated Marginal Ice Zone (MIZ), defined as the region experiencing most recent sea-ice melting/retreat, across MIS5e is particularly interesting because the MIZ is the region in the Southern Ocean with the highest summer PP (Fitch and Moore, 2007; Arrigo et al., 2008). The latitudinal position of the summer sea-ice edge is therefore important for the size of the high-productivity area associated with the MIZ. Changes in the position of the sea-ice edge in the late Pleistocene have affected the total Southern Ocean PP, as is clear from paleoproductivity reconstructions: PP was enhanced north of the Polar Front (PF) during glacial times, and south of the PF during interglacial times (Mortlock et al., 1991). A shift of the summer sea-ice edge (SSE) towards higher latitudes or changes in the size of the MIZ will also likely affect PP in the future (Sarmiento et al., 2004; Arrigo et al., 2008; Deppeler and Davidson, 2017). However, many Southern Ocean sea-ice reconstructions have focused on the winter sea ice edge (WSE) during glacial times instead (Gersonde and Zielinski, 2000; Bianchi and Gersonde, 2002; Howe et al., 2002; Crosta et al., 2004; Gersonde et al., 2005; Ferry et al., 2015), because sea ice expansion and related stratification have been proposed as a mechanism for glacial CO_2 reduction by prohibiting the air-sea CO_2 exchange during glacial periods (Stephens and Keeling, 2000; Sigman et al., 2004, 2010, 2021,; Martínez-Garcia et al., 2009; Ferrari et al., 2014).

In this paper we use sediment core AS05-10 collected off the Ross Sea continental slope (Fig. 1) to reconstruct the position of the SSE and the MIZ over the late Pleistocene glacial-interglacials and its influence on PP in the Adare Basin. The core is studied at high resolution (1–3 cm intervals) with paleobiological (diatoms, dinoflagellate cysts, benthic foraminifera), geochemical and sedimentological proxies. It straddles an interval between ~350 and 70 ka (see the age model below and Supplementary Information) and thus allows reconstructing and comparing the stepwise evolution of each glacial and interglacial stage.

High-resolution records close to the Antarctic margin, covering multiple glacial and interglacial stages have only become available over the last decade (Hillenbrand et al., 2009; Xiao et al., 2016; Wilson et al., 2018), but none are from the Ross Sea area. With only one previously published low-resolution record from the Ross Sea (Ceccaroni et al., 1998), the record of AS05-10 thus substantially increases our knowledge on sea-ice variability and paleoproductivity for this area on glacial-interglacial timescales.

1.1. Oceanographic and geological setting

Core AS05-10 was drilled at the continental slope offshore the Drygalski Basin, which is called the Adare Basin, western Ross Sea (173.065°E, 70.835°S), at a water depth of 2377 m (Fig. 1) during the XX Antarctic Italian Cruise (01/15/2005-02/27/2005). Investigations are within the frame of the PNRA (Antarctic Italian National Research Program) projects 2004/4.08 "Bottom water production in the Ross Sea during the Late Quaternary: a geochemical and micropaleontological study" and 2009/A2.01 "Sub-milankovian paleoclimatic variations and deep circulation

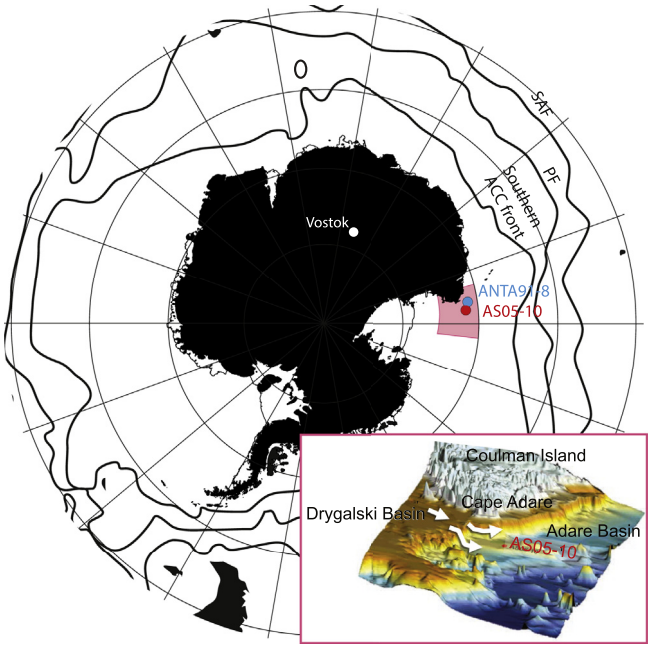

Fig. 1. Map of the study site. Details of the bathymetry and topography of the pink area are shown. ACC front = Antarctic Circumpolar Current front; PF = Polar Front; SAF = Subantarctic Front (Orsi et al., 1995). (For interpretation of the references to color in this figure legend, the reader is referred to the Web version of this article.)

linkages during the Late Quaternary (MIS 5–7) in the Ross Sea slope (Antarctica)".

Today, the drill site of core AS05-10 is overlain by Circumpolar Deep Water (CDW) (Orsi and Wiederwohl, 2009), and influenced by occasional gravity currents that flow along the Drygalski Basin slope (Gordon et al., 2009). These gravity currents form through local mixing of relatively warm oceanic thermocline waters with relatively cold Modified CDW (MCDW; CDW that has been mixed with Ross Sea shelf waters) and High Salinity Shelf Water (HSSW) (Orsi and Wiederwohl, 2009). This very dense HSSW forms in the western sector of the Ross Sea as a result of the ongoing formation and removal of new sea ice in the Terra Nova Bay Polynya (Jacobs et al., 1985; Budillon et al., 1999), due to strong katabatic winter winds blowing over the Ross Ice Shelf (Bromwich and Kurtz, 1984). HSSW flows northward over the shelf and mixes with surface waters and MCDW at the shelf edge to form Antarctic Bottom Water (AABW) (Jacobs et al., 1970; Jacobs, 1991; Budillon et al., 2002, 2003; Bergamasco et al., 2004; Orsi and Wiederwohl, 2009). Surface and shelf waters in the Ross Sea are characterized by relatively high oxygen concentrations and low dissolved silica (DSi), and also determine the oxygen and DSi concentrations of the HSSW and AABW through bottom-water formation (Jacobs, 1989). Submarine canyons and basins, such as the Drygalski Basin, serve as conduits for bottom-water formation (Jacobs, 1989; Davey and Jacobs, 2007).

Spring warming and seaward winds cause northward sea ice retreat along the western Ross Sea coast (Spreen et al., 2008; Smith et al., 2012), while the offshore sea-ice melt-back progresses southward. These two open water systems connect early January (Spreen et al., 2008), so that, by definition, the Marginal Ice Zone (MIZ) is overlying AS05-10 in January (Fitch and Moore, 2007). Water column stratification, low wind speeds and nutrient release after sea-ice retreat trigger large phytoplankton blooms (Fitch and Moore, 2007; Arrigo et al., 2008; Smith et al., 2012). Together with the MIZ, the Ross Sea shelf surface waters are among the most productive areas of the Southern Ocean, with the shelf area alone contributing one third of the Southern Ocean total primary production (PP) (Arrigo et al., 2008; Smith et al., 2012). *Phaeocystis antarctica*, which is able to maintain high photosynthetic rates in the deeply-mixed Ross Sea polynya (Arrigo et al., 1999, 2003; Sedwick et al., 2000; Peloquin and Smith, 2007), is responsible for the bulk of this high PP. However, when surface waters stratify due to the melting sea ice in summer, diatoms replace *P. antarctica* (Arrigo et al., 1999, 2003), taking advantage of the iron release from the melting sea ice (Arrigo et al., 2003; De Jong et al., 2013; McGillicuddy et al., 2015). Similar to today, the surface waters of Site AS05–10 may have experienced shifts towards diatom-dominated PP during past interglacials.

About 90% of the total carbon and 30% of total biogenic silica production by *P. antarctica* and diatom blooms is seasonally recycled in the upper water column (Nelson et al., 1996). Still, organic carbon (OC) and biogenic silica (BSi) export to the seafloor is large in the Ross Sea, but varies strongly between years (Nelson et al., 1996; Smith. et al., 2011) and regions (Nelson et al., 1996). OC export in the central Ross Sea occurs mainly through aggregate and fecal pellet formation (Asper and Smith, 1999; Smith et al., 2011). While high sinking rates of these fecal pellets imply that most sedimentary OC originated from the surface waters overlying Site AS05-10, part is shown to be derived from resuspended sediments from shallow banks (Nelson et al., 1996) through gravity flows (Gordon et al., 2009). Out of all the material that reaches the Ross Sea floor, another ~95% of OC and 80% of BSi gets remineralized (Nelson et al., 1996) under the influence of the high-oxygen low-DSi bottom waters (Jacobs, 1989).

2. Material

Core AS05-10 recovered 750 cm of fine-grained sediment. The top 40 cm is an alternation of brown and yellow clays; the rest of the core is homogeneous greyish clay with occasional clasts (>1 cm) (Fig. 2). The core has always been kept at −20 °C. At ISMAR-CNR Bologna laboratory the sections of the core have been subsequently cut frozen in slices ca. 1 cm thick (Asioli and Langone, 2010).

Construction of the age model and terminology used.

Comparison between the whole-core magnetic susceptibility (MS) in core AS05-10 and in the nearby core ANTA91-8 (Fig. 1 for its location) previously published at lower resolution (Ceccaroni et al., 1998) suggests our core contains at least MIS5 and MIS7.

We studied the section between 180 and 750 cm below sea floor (cmbsf) at high resolution and constructed an age model for this interval. The age model is based on two diatom datums: the last occurrence (LO) of *Rouxia leventerae* (0.138 Ma; the end of MIS6; Xiao et al., 2016) at about 388 ± 20 cmbsf; and the LO of *Rouxia constricta* (0.28 Ma; mid-MIS8; Zielinski and Gersonde, 2002) at about 594 ± 19 cmbsf. The position of Termination I (18–11.5 ka) was estimated from a marked decrease in the %BSi and a sharp increase in the MS record between 115 and 147 cmbsf (see Supplementary Information).

The cyclic behavior of measured parameters in core AS05-10 have been used to improve dating by correlating these cycles to known orbital parameters and glacial-interglacial cyclicity. In the Southern Ocean records south of the Polar Front (PF), cycles of biogenic barium (Ba_{bio}) and %BSi are tightly linked, representing glacial-interglacial changes in PP with higher values during the interglacials (Shimmield et al., 1994; Bonn et al., 1998; Pudsey and Howe, 1998; Hillenbrand and Fütterer, 2001; Hillenbrand et al., 2003, 2009; Wilson et al., 2018). Other geochemical elements have also shown a relation with glacial-interglacial variation related to provenance or terrigenous supply (Bertram et al., 2018; Jimenez-Espejo et al., 2020). In several other Southern Ocean records, glacial-interglacial cyclicity has been observed in MS: high BSi production dilutes lithogenic detritus input, which results in anti-correlation of MS with BSi (and Ba_{bio}) (Hillenbrand et al., 2009; Collins et al., 2012; Xiao et al., 2016). In addition, some siliceous microfossils, such as the diatom *Eucampia antarctica*, show cyclic glacial-interglacial variation in relative abundance (Burckle and Cooke, 1983; Burckle and Burak, 1988; Collins et al., 2012; Xiao et al., 2016).

To build an age model for core AS05-10, we have tested several proxies for orbitally-driven cyclicity, using the diatom event datums and the position of Termination I for a first-order age model (see Suppl. Inf.). Successively, the Ti/Al record was used to tune core AS05-10 to the 19-kyr precession by using evolutive harmonic analysis (EHA) and evolutive spectral misfit analysis (e-ASM) of the Astrochron program in R (Meyers and Sageman, 2007; Meyers et al., 2012). The Ti/Al record was chosen as the cyclicities obtained from this record matched the expected astronomical cycle lengths based on the microfossil occurrence datums best. In addition, Al and Ti are found mainly in aluminosilicates and heavy minerals (Calvert and Pedersen, 2007), although both elements can be concentrated in diatom frustules, which means that at site AS05-10 the Ti/Al is likely influenced by the diatom export productivity in addition to a lithogenic signal. Nevertheless, Ti and Al are poorly mobilized during diagenesis, which means this proxy is least susceptible to changes in post-depositional remobilization and/or bottom-water oxygenation in comparison to for example Ba_{bio} and BSi. A final age model was obtained by tuning the obliquity pacing in the Ti/Al record to that within the deuterium-based air temperature reconstructions (ΔT_s) of the Vostok ice core (Petit et al., 1999). The Vostok ice core ΔT_s age model is based on the Antarctic Ice Core

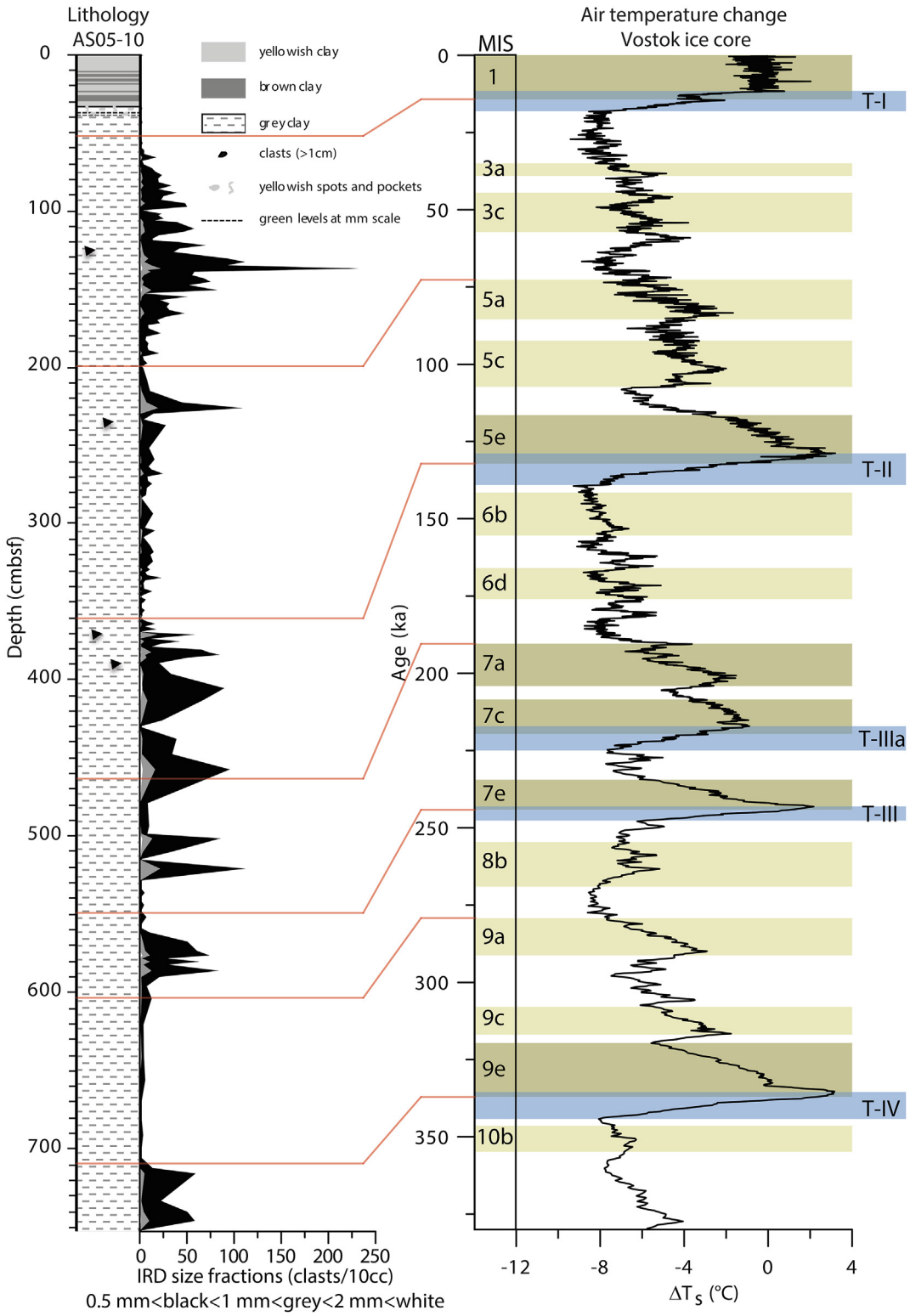

Fig. 2. Lithology of core AS05-10, including IRD (left). Relative air temperature change recorded in the Vostok ice core (Petit et al., 1999). The dark and light shaded areas mark the interglacials versus the interstadials, respectively, following Past Interglacials Working Group of PAGES (2016) with nomenclature following Railsback et al. (2015). Terminations (T) are marked in blue. Red lines mark the position of the onset of each Marine Isotope Stages (MIS) within the lithology based on the age model (Suppl. Inf.). (For interpretation of the references to color in this figure legend, the reader is referred to the Web version of this article.)

Chronology (AICC2012), which is based on a multi-proxy synchronization of multiple ice cores (Bazin et al., 2013; Veres et al., 2013). In our approach, we note that the 19-kyr precession signal within the Ti/Al record follows the precession signal of local (70.8°S) insolation (see Suppl. Inf.).

Names and ages for the individual marine isotope stages and glacial terminations were adopted from Railsback et al. (2015). Notably, this results in the designation of MIS9a to what is also

known as MIS8.5. The relation between our stratigraphic record, the marine isotope stages according to Railsback et al. (2015), the ΔT_s record from the Vostok ice core, and the glacial Terminations in the ΔT_s record is shown in Fig. 2.

Core AS05-10 continuously covers an interval between ~350 and 70 ka and thus allows reconstructing oceanographic conditions of each glacial and interglacial stage in that interval and comparing the late Pleistocene interglacials. The definition of an interglacial is based on the comparative study of interglacials of the past 800 kyr by the Past Interglacials Working Group of PAGES (2016). Interglacials thus include MIS 9e, 7e, 7a-c and 5e. Following Cheng et al. (2009), the glacial Termination prior to MIS7a-c is termed Termination IIIa. We use the terms '(glacial) Termination' and '(onset of) Marine Isotope Stage, MIS' as the rapid shift from a glacial to an interglacial period marked by the steep temperature shift recorded in the Vostok ice core. The term 'glacial-interglacial transition' indicates the environmental changes related to the transition from a cold to a warm period, not necessarily synchronous to the Termination. We will describe several phases of each glacial-interglacial transition based on the proxy data.

3. Methods and proxy interpretations

3.1. Magnetic susceptibility

The gravity core AS05-10 was frozen at −20 °C immediately after collection and scanned onboard for the magnetic susceptibility by means of a Bartington ring sensor for whole-core magnetic susceptibility with measurements at 2-cm steps.

Magnetic susceptibility is determined by the grain size and concentration of ferromagnetic minerals, which is determined by the source of the terrigenous material as well as the degree of dilution by biogenic input (Pudsey and Howe, 1998; Collins et al., 2012). Magnetic susceptibility has been used to correlate marine sediment cores as well as ice cores on glacial-interglacial timescales (Pudsey and Camerlenghi, 1998; Pudsey and Howe, 1998; Pugh et al., 2009; Xiao et al., 2016).

3.2. X-ray fluorescence analyses

Geochemical analyses of 255 bulk sediment samples have been performed by X-ray fluorescence (XRF) located at the Department of Geosciences of Padova University (Italy). Dried sediment samples (1.5 g) were ground with an agate mortar and fused with lithium tetraborate (1:10; sample:lithium tetraborate). The obtained panes were analyzed with a Philips PW2400 spectrometer to measure the concentrations of the chemical elements by using several international geologic standards. Loss on ignition (LOI) was measured after heating samples to 980 °C. The instrumental precision is within 0.6% for the major elements and within 3% for trace elements.

Subsequently, biogenic barium (Ba_{bio}) was calculated as the concentration of barium exceeding the detrital contribution observed in shales (Dymond et al., 1992). Barium is generally considered a proxy for paleoproductivity (Bonn et al., 1998; Ceccaroni et al., 1998; Pudsey and Howe, 1998; Hillenbrand et al., 2003, 2009; Xiao et al., 2016). However, in some cases barium records are influenced by detrital input (Klump et al., 2000) and/or changes in redox conditions (McManus et al., 1998). To account for this, elemental ratios considered in this paper are V/Cr, Ni/Co, and U/Th, which are indicative of bottom water oxygenation (Jones and Manning, 1994), and Zr/Rb, which reflects the relative grain size (Dypvik and Harris, 2001) of the sediments and is indicative of increased detrital input at a lower shelf setting such as AS05-10. Because of low uranium concentrations a cut-off value of 2 ppm for was used for uranium to construct the U/Th record.

3.3. Biogenic silica

Biogenic silica was measured on 162 samples at ISMAR-CNR Bologna, following the dissolution method of DeMaster (1981) and the colorimetric analysis of Strickland and Parsons (1972) using a 0.5 M NaOH solution as extracting agent with an uncertainty of about 10%. °C.

Changes in paleoproductivity in the Southern Ocean have been determined by measuring biogenic silica (BSi) (Shimmield et al., 1994; Ceccaroni et al., 1998; Bonn et al., 1998; Pudsey and Howe, 1998; Hillenbrand and Fütterer, 2001; Hillenbrand et al. 2003, 2009; Xiao et al., 2016), often in combination with Ba_{bio}. Here, BSi is also considered a proxy for paleoproductivity.

3.4. Organic carbon, total nitrogen and $\delta^{15}N$

Total organic carbon (OC) and total nitrogen (TN) contents, and their stable isotope compositions were measured at ISMAR-CNR Bologna on 2 different aliquotes by a Finnigan DeltaPlus XP mass spectrometer directly coupled to a FISONS NA2000 Element Analyzer via a Conflo III interface for continuous flow measurements (Tesi et al., 2007). Samples for OC analysis were first decarbonated in silver capsules after acid treatment (HCl 1.5 M). Samples for OC and TN contents and $\delta^{15}N$ were weighted in tin capsules and directly inserted in the EA autosampler. The average standard deviation of each measurement, determined by replicate analyses of the same sample, was ±0.07% for OC and ±0.009% for TN. The isotopic composition of nitrogen is presented in the conventional δ notation and reported as parts per thousand (‰). The internal standard for ^{15}N isotopic measurements was IAEA-N-1 (ammonium sulfate, +0.4‰ vs. air). Errors for replicate analyses of the standards were ±0.2‰.

The %OC and %TN in the sediments reflect the relative abundance in weight percentage of organic matter in the sediments. High %OC and %TN could either be the result of increased primary productivity or increased preservation.

Nitrogen fractionation by phytoplankton in the surface waters due to preferred uptake of ^{14}N over ^{15}N, makes $\delta^{15}N$ a proxy for surface water nutrient utilization; utilization being the ratio between phytoplankton uptake and nutrient supply (Altabet and Francois, 1994, 2001). The higher the $\delta^{15}N$ value, the higher the nutrient utilization is. Post-depositional alteration of the $\delta^{15}N$ value due to early diagenesis at the sediment-water interface may, however, result in an increase of the bulk $\delta^{15}N$ value in the sediments, particularly at oxic pelagic sites with low accumulation rates (Robinson et al., 2012). However, empirical data across a range of sedimentation rates and sediment compositions at different water depths, suggest that even in slowly accumulating regions the study site bulk sedimentary $\delta^{15}N$ records will primarily reflect changes in the $\delta^{15}N$ of exported nitrogen in most cases. For example, in sediments with poor organic matter preservation, such as the Mediterranean marls (Higgins et al., 2010), or in millions-of-years-old sediments, such as the Cretaceous black shales (Higgins et al., 2012), the bulk $\delta^{15}N$ values are indicative of the biogeochemical cycling of nitrogen. Nevertheless, a bias due to the presence of inorganic nitrogen or input of terrestrial organics can be detected in a %OC-versus-%TN plot as a nonzero y-intercept of the linear regression line (Robinson et al., 2012).

3.5. Archaeal lipid (GDGT) processing and analyses

A total of 39 samples covering the period between 90 and 313 ka (243–665 cmbsf) were processed for analysis of glycerol dialkyl glycerol tetraethers (GDGTs) to derive TEX_{86}-based temperatures (Schouten et al., 2002). Sample processing involved extraction of

freeze-dried and manual powdered sediments through accelerated solvent extraction (ASE; with dichloromethane (DCM)/methanol (MeOH) mixture, 9:1 v/v, at 100 °C and 7.6 × 10^6 Pa). The polar GDGTs were separated from non-polar molecules through Al_2O_3 column chromatography using hexane/DCM (9:1, v/v), hexane/DCM (1:1, v/v) and DCM/MeOH (1:1, v/v) for separating apolar, ketone and polar fractions, respectively. The polar fractions were dried under N_2, dissolved in hexane/isopropanol (99:1, v/v) and filtered through a 0.45 μm 4 mm diameter polytetrafluorethylene filter. After that, the dissolved polar fractions were injected and analyzed by ultra-high performance liquid chromatography/mass spectrometry (UHPLC/MS) at Utrecht University according to the method described by Hopmans et al. (2016). GDGT chromatogram peaks were integrated using Chemstation software. All samples containing low concentrations of GDGT-3 (below 3*10^3 mV) were not used for TEX_{86}-based temperature reconstructions and Branched and Isoprenoid Tetraether (BIT) index calculations (Hopmans et al., 2004).

For the TEX_{86}-based subsurface sea water temperature reconstruction we used the BAYSPAR calibration of Tierney and Tingley (2014), which gives a depth-integrated temperature estimate for the top 200 m of the surface water column based on surface sediment samples with a 90% confidence interval based on a linear regression with a slope and intercept specific for the region (a 20 ° × 20 ° grid box) of our study. We have chosen this calibration as Thaumarchaeota are virtually absent in the upper 0–45 m (Kalanetra et al., 2009), and reconstructed temperatures thus likely reflect a subsurface signal (Kim et al., 2012). Based on Tierney and Tingley (2015), the expected slope and intercept of the TEX_{86}-subT calibration curve for our study area are 0.012 and 0.37 respectively, with a standard error (1σ) of 7.2 °C. The standard error depends on the number of core tops used in the calibration. The number of available surface sediment samples used in the calibration at high southern latitude is low, which gives a high standard error. Despite this, reconstructed trends are reliable, as globally there is little variation in slope (values between 0.005 and 0.016) and intercept (values between 0.3 and 0.4) (Tierney and Tingley, 2015).

The (expected) normal pelagic marine distribution of isoprenoideal GDGTs (iGDGTs) in the sediments, and therefore TEX_{86} values, can be affected by the iGDGT input of methanogenic or methanotrophic archaea (Koga et al., 1998), or other non-temperature related biases, such as archaeal growth phase (Elling et al., 2014), oxygen concentrations (Qin et al., 2015), and ammonia oxidation rates (Hurley et al., 2016). To search for possible biases, several indices have been developed, which we applied to our samples. These include the methane index (MI) (Zhang et al., 2011), the GDGT-0/crenarchaeol ratio (Blaga et al., 2009; Sinninghe Damsté et al., 2009), the GDGT-2/crenarchaeol ratio (Weijers et al., 2011) and the Ring Index (|ΔRI|) (Zhang et al., 2016) (Suppl. Table S1).

In addition, we explore other proxies related to *in situ* production of branched GDGTs (brGDGTs). While initially considered purely soil-derived (Hopmans et al., 2004; Dearing Crampton-Flood et al., 2019), it was subsequently shown that brGDGTs are also produced within marine sediments (Peterse et al., 2009) and the water column (Zell et al., 2014). The relative abundance of brGDGTs versus iGDGTs is known as the BIT index, which is defined as (brGDGT-I + brGDGT-II + brGDGT-III)/(brGDGT-I + brGDGT-II + brGDGT-III + Crenarchaeol) (Hopmans et al., 2004). Other proxies based on brGDGTs, such as the degree of cyclization, have been suggested as indicators of *in-situ* sedimentary GDGT production versus soil-derived input of brGDGTs (Weijers et al., 2014; Sinninghe Damsté, 2016). The degree of cyclization within tetramethylated brGDGTs is called $\#rings_{tetra}$, is defined as ([brGDGT-Ib]+2*[brGDGT-Ic])/([brGDGT-Ia]+[brGDGT-Ib]+[brGDGT-Ic]) (Sinninghe Damsté, 2016) and is particularly varying as a function of *in situ* production.

3.6. Palynology

A total of 49 samples taken between 71 and 313 ka (195 and 665 cmbsf) were prepared for examination of palynomorphs by using established palynological processing methods. Samples were freeze-dried and a known amount of *Lycopodium clavatum* spores was added to c.a. 10 g of material. Samples were treated with 30% HCl to remove the carbonates and with 38% cold HF to remove silicates. After each acid treatment, samples were washed with water, left standing for 24 h to let the material settle, and subsequently decanted. The HF treatment included 2 h of shaking at ~250 rpm and adding of 30% HCl to remove fluoride gels. The residue was then sieved through a 10-μm mesh sieve and subsequently placed in an ultrasonic bath to break up clumps of organic matter and removal of heavy minerals. The remaining material was concentrated in ~1 ml of glycerin water used to make microscope slides. At least 200 dinoflagellate cysts were counted for each sample, if possible.

Dinoflagellate cysts can be used for reconstructing the presence of sea-ice (de Vernal and Hillaire-Marcel, 2000; Esper and Zonneveld, 2007; Bonnet et al., 2010; De Vernal et al., 2013) and primary productivity (Radi and de Vernal, 2008; Prebble et al., 2013). Moreover, based on the link between dinoflagellate cyst assemblages and the Antarctic and Polar Front Zones (Marret and De Vernal, 1997; Marret et al., 2001; Esper and Zonneveld, 2002; Prebble et al., 2013), dinoflagellate cysts have been used as an indicator of glacial-interglacial shifts of the Polar Front (Howe et al., 2002; Esper and Zonneveld, 2007). Dinoflagellate cysts are here grouped in gonyaulacoid and protoperidinioid. It has been shown by infrared analysis that the cyst wall chemistry of phototrophic usually transparent gonyaulacoid dinoflagellates is distinctly different from that of the brown, heterotrophic protoperidinioids, and probably determined by the different feeding strategy of the dinoflagellates that produced the cyst (Ellegaard et al., 2013). Abundances of gonyaulacoid dinoflagellate cysts are typically less than 20% in surface sediments south of the PF and mostly represented by *Impagidinium pallidum* (Marret and De Vernal, 1997; Esper and Zonneveld, 2007; Prebble et al., 2013; Marret et al., 2019). High abundances of *I. pallidum* are associated with seasonal sea-ice in both the Arctic and Antarctic (Marret and De Vernal, 1997; De Vernal et al., 2001; Kunz-Pirrung et al., 2001; Esper and Zonneveld, 2007; Bonnet et al., 2010; Pieńkowski et al., 2013; Zonneveld et al., 2013; Marret et al., 2019). Around Antarctica it is most dominant in nutrient-rich waters south of the PF and the seasonal sea-ice zone (SSIZ) upon seasonal melting of sea ice (Marret and De Vernal, 1997; Marret et al., 2001; Esper and Zonneveld, 2007).

Protoperidinoid cysts are dominant in present-day Subantarctic and Antarctic surface sediments where sea ice coverage and productivity are high (Marret and De Vernal, 1997; Esper and Zonneveld, 2002; Pieńkowski et al., 2013; Prebble et al., 2013; Zonneveld et al., 2013). Protoperidinioid cysts are more sensitive than gonyaulacoid cysts to degradation in oxic environments (Versteegh and Zonneveld, 2002; Zonneveld et al., 2010). High abundances of protoperidinioid cysts in an assemblage could be representative of a high primary productivity environment as well as decreased bottom water oxygenation, which enhances their preservation. A way to at least partially circumvent this bias is the use of the concentration of protoperidinioid cysts (cysts/gram sediment) and/or of total dinocysts as proxy for primary productivity (Reichart and Brinkhuis, 2003).

Other palynomorphs considered here include the gymnodinioid dinoflagellate cyst *Gymnodinium* spp., the prasinophycean alga *Cymatiosphaera* spp. and the acritarch *Leiosphaeridia* spp. *Cymatiosphaera* spp. is considered to be the phycoma of the chlorophyte *Pterosperma* (Mudie et al., 2010; Hartman et al., 2018a). *Gymnodinium* spp., *Cymatiosphaera* spp. and *Leiosphaeridia* spp. have all been associated with surface water stratification due to fresh(melt) water (Mudie, 1992; Hannah, 2006; Warny et al., 2006, 2016; Ribeiro et al., 2016; Hartman et al., 2018a).

3.7. Benthic foraminifers

The 103 samples between 180 and 578 cmbsf were treated in the laboratory for the analysis of foraminiferal assemblages and IRD. The samples were washed with a 0.063-mm mesh sieve, and thoroughly examined while they were wet with Leica M165C (11.7-192×) reflective optical stereomicroscope. The distribution of foraminifers is expressed in terms of absolute abundances (number of individuals/10 cc).

Benthic foraminifera are indicative of export productivity from the surface waters to the sea floor (Jorissen et al., 1995, 2007Jorissen et al., 1995, 2007; Thomas and Gooday, 1996). Here, two species of benthic foraminifer are considered: *Martinottiella nodulosa* and *Eggerella bradyi*. These species have been reported at nearby surface sediment sample sites and core sites (Asioli, 1995; Barbieri et al., 1999). The occurrence of *M. nodulosa* seems to be linked to the availability of well-sorted quartz grains that it needs for constructing its test (Lindenberg and Auras, 1984). *M. nodulosa* is likely an infaunal species as its close relative, *Martinottiella communis*, has been shown to live at 1–3 cm sediment depth (Sabbatini et al., 2004). *E. bradyi* appears to be epifaunal with occurrences of living specimens in the 0–0.5 cm depth range (Asioli, 1995; Asioli and Langone, 2010).

3.8. Ice rafted debris (IRD)

The fraction larger than 0.500 mm in the 120 samples washed for foraminifera were dried and examined for IRD content with the same microscope used for the foraminifer study. Three fractions were chosen (>2 mm, 1–2 mm, and 0.5–1 mm), counting only the lithic clasts and excluding all remains of organisms. The content of the three fractions is expressed as a concentration (number of clasts/10 cc).

IRD is indicative of icebergs reaching the depositional site and thus can be expected at ice-proximal sites. In the North Atlantic, high concentrations have been associated with glacial collapse as well as ice sheet growth (Heinrich, 1988; Cofaigh, 2012). Around Antarctica, however, a relation between glacial collapse and IRD is not as evident as in the northern hemisphere (Cofaigh, 2012) and in some records lags glacial Terminations (Grobe and Mackensen, 1992). Notably, increased IRD concentrations can simply be the result of decreased sedimentation rates and winnowing (Cofaigh et al., 2001). However, in the absence of high-energy bottom currents, increased IRD concentrations deposited in hemipelagic muds with biogenic material have been related to both periods of ice sheet advance and periods of intense calving and ice-shelf break-up around the Antarctic Peninsula (Pudsey and Camerlenghi, 1998; Lucchi et al., 2002; Minzoni et al., 2015). Furthermore, IRD layers have been associated with rapid ice-shelf break-up of the George VI ice shelf and associated iceberg release during the Holocene (Bentley et al., 2005).

3.9. Diatoms

Diatoms were processed according to the standard method, as described by Bernárdez et al. (2008) and Rigual-Hernández et al. (2017). A fixed amount of 0.5 g of sediment was placed in 600 ml beakers and treated with HCl and H_2O_2 in order to remove carbonate and organic matter. Bi-distilled water was added and left to settle over a night. The excess of liquid was removed with a vacuum pump. This process was repeated several times, until a neutral pH was achieved. For each sample, total volume and suspension volume used to mount the slides were known. For slide preparation, suspension was strewn evenly onto cleaned 18 × 18 mm cover slips placed in a Petri dish, after stirring the solution for homogenization. Slides were mounted with a toluene based synthetic resin mounting medium (Permount™, Fisher Scientific).

A total of 193 samples was analyzed at Salamanca University using a Leica DMLB microscope with phase contrast illumination at ×1000 magnification for counting diatoms. Samples have been taken about every 5 cm, except for the interval between 428 and 472 cmbsf (168–197 ka), where sample spacing is about 10 cm, followed by a gap between 472 and 518 cmbsf (197–225 ka). The counts were performed following the method of Schrader and Gersonde (1978). A minimum of 400 valves was counted for each sample, where possible. For samples with a high amount of *Chaetoceros* resting spores (RS) at least 100 valves of non-dominant taxa were counted (Schrader and Gersonde, 1978). The state of preservation of the fossil association was estimated by visual examination.

Diatom relative abundances are used to reconstruct sea-ice and temperatures in Southern Ocean sedimentary records (e.g., Bárcena et al., 1998, 2002; Crosta et al., 2008; Denis et al., 2010; Esper and Gersonde, 2014). To be able to reconstruct sea-ice dynamics in this study, species with the same cryophylic and open-ocean ecological requirements were grouped: the seasonal sea-ice group and open-ocean group, respectively. Other species that are considered here are *Eucampia antarctica*, *Chaetoceros* resting spores (RS), *Fragilariopsis rhombica* and *Fragilariopsis kerguelensis*.

E. antarctica is a proxy for sea-ice cover, as it forms long chains of diatom valves during winter or in areas with extensive sea-ice cover (Kaczmarska et al., 1993). In the Atlantic sector of the Southern Ocean, percentages in surface sediment samples south of the SSE lie between 5 and 12.5% (Esper et al., 2010). Although increased abundances of *E. antarctica* have been associated with surface water temperatures up to 5.5 °C within the Polar Frontal and Subantarctic Frontal Zones (Zielinski and Gersonde, 1997; Esper et al., 2010), this is likely because no distinction was made between *E. antarctica* var. *antarctica* and *E. antarctica* var. *recta*, the former being associated with the SSIZ (Fryxell and Prasad, 1990; Esper et al., 2010). As of yet, a sediment distribution pattern for the two varieties for the Southern Ocean has to be documented (Armand et al., 2005, 2008). However, based on a study of the Amundsen and Weddell Seas the distribution of the two varieties offer a promising potential as quantitative proxy for austral summer SSTs (Allen, 2014). This study shows that core tops with high relative abundances of *E. antarctica*, as well as relatively high amounts of symmetrical and terminal valves, typical for the short colonies of *E. antarctica* var. *recta*, are associated with SSTs below 0.5 °C and 10–12 months sea-ice cover (Allen, 2014).

In today's surface sediments *Chaetoceros* valves and RS show a bimodal distribution, because *Chaetoceros* species do not all have the same environmental preferences (Esper et al., 2010). Although certain species of *Chaetoceros* prefer near shore sea-ice environments (Garibotti et al., 2005), fossil Pleistocene *Chaetoceros* RS cannot easily be distinguished at species level (Gersonde and Zielinski, 2000; Esper et al., 2010), making them unsuitable as a proxy for sea ice. Generally, however, high percentages of *Chaetoceros* RS are associated with stratification of the surface waters, either through glacial runoff and sea-ice melting close to the

Antarctic margin or through iceberg melting in the open ocean (Crosta et al., 1997). *Chaetoceros* subgenus *Hyalochaete* is known to overwinter in sea ice and may be able to seed the water column once the sea ice melts, leading to early-season blooms until nutrients are depleted (Alley et al., 2018). The formation of *Chaetoceros* RS is typically associated with nutrient depletion after phytoplankton blooms (Leventer et al., 1996). The highly silicified RS are highly resistant to water column and surface sediment dissolution (Crosta et al., 1997) and sink rapidly down the water column, thereby avoiding grazing (Rembauville et al., 2015). This makes them important contributors to carbon export to the ocean floor (Rembauville et al., 2016).

The seasonal sea-ice group is composed of *Fragilariopsis curta*, *F. cylindriformis*, *F. cylindrus*, *F. obliquecostata*, *F. ritscheii*, *F. sublinearis*, and *F. vanheurkii*, which are all commonly found in the sea ice and highest in abundance (more than 20%) in surface sediments close to the summer sea-ice edge (SSE) with 9–11 months/yr sea-ice cover (e.g., Gersonde and Zielinski, 2000; Armand et al., 2005; Esper et al., 2010). The diatom species within the seasonal sea-ice group, such as *F. curta* and *F. cylindrus*, bloom during late summer and dominate the surface waters south of the PF and are particularly associated with the MIZ (Gersonde and Zielinski, 2000; Grigorov et al., 2014; Malinverno et al., 2016). It has been suggested that in an upper water column that is stabilized by the overlying meltwater lens from melting sea ice, *F. curta* and other seasonal sea-ice diatoms have an advantage over other diatoms due to a combination of their small size and low settling rates, while other species require mixing to stay in suspension (Leventer, 1998). However, because these seasonal sea-ice diatoms are very susceptible to dissolution (Grigorov et al., 2014), abundances are relatively low in the surface sediments underlying the high-productivity surface waters. Generally, their abundances increase towards Antarctica, which makes them good indicators of high annual sea-ice cover (Zielinski and Gersonde, 1997; Bárcena et al., 1998, 2002; Bárcena et al., 1998, 2002; Gersonde and Zielinski, 2000; Armand et al., 2005), also within fossil diatom records (Leventer et al., 1996; Leventer, 1998; Gersonde and Zielinski, 2000; Gersonde et al., 2003; Crosta et al., 2007, 2008; Riesselman and Dunbar, 2013). In particular, relative abundances of 3% *F. curta* and *F. cylindrus* have been used to trace the WSE in various Southern Ocean sediment cores (Gersonde and Zielinski, 2000; Bianchi and Gersonde, 2002).

F. rhombica is considered separately from the other seasonal sea-ice diatoms. Although generally very low in abundance in modern surface sediments, this species shows relatively highest abundances within the SSIZ, preferring slightly warmer summer SSTs in comparison to *F. curta* (Armand et al., 2005; Esper et al., 2010). An increased abundance of *F. rhombica* with respect to *F. curta* has been interpreted as a reduced competitiveness of *F. curta* due to slightly warmer temperatures and/or a reduction of sea ice during spring/summer (Denis et al., 2006; Crosta et al., 2007, 2008).

In Southern Ocean surface sediments, *F. kerguelensis* can be found in highest abundances north of the SSE (Crosta et al., 2005a). Surface-sediment abundances of *F. kerguelensis* increase sharply when summer SSTs reach values above 1 °C (Crosta et al., 2005a, 2007). Instead, surface-sediment abundances of *F. curta* decrease sharply when summer SSTs reach values above 1 °C (Armand et al., 2005), which is the reason that shifts between *F. curta* and *F. kerguelensis* have been interpreted as SST change (Crosta et al., 2007). Furthermore, high (>20%) surface-sediment abundances of *F. kerguelensis* are associated with <9 months of annual sea-ice cover, while highest abundances of *F. curta* (20–30% in the Ross Sea sector of the Southern Ocean) are found between 9 and 11 months of sea ice (Armand et al., 2005; Crosta et al., 2005a). The shift in dominance between these two species therefore seems to mark the position of the SSE (Esper et al., 2010; Esper and Gersonde, 2014).

The open-ocean group is composed of *Thalassiosira eccentrica*, *Shionodiscus gracilis* (=*Thalassiosira gracilis*), *T. lentiginosa*, *Shionodiscus oestrupii*, *T. oliverana*, and *T. tumida*, as the genus *Thalassiosira* is typically associated with open water conditions (generally less than 4 months sea ice per year) during the growing season (Johansen and Fryxell, 1985; Crosta et al., 2005a; Campagne et al., 2016). However, differences between species within this group are important for our study. Highest relative abundances (>8%) of *S. gracilis* are particularly found in surface sediments underlying the SSIZ where it prefers much higher sea-ice conditions, while highest relative abundances (>12%) of *T. lentiginosa* (and highest relative abundances of other *Thalassiosira* species) are found north of the WSE (Esper et al., 2010). Notably, *Thalassiosira* species in general show increased relative abundances within the sediments when summer SSTs lie above ~1 °C, with the exception of *S. gracilis* which is associated with summer SSTs lying between −1 °C and 1 °C (Crosta et al., 2005a; Esper et al., 2010).

4. Results

4.1. Magnetic susceptibility

Pronounced magnetic susceptibility (MS) minima correspond to pronounced biogenic silica (BSi) maxima, which precede each interglacial stage (Suppl. Fig. S1). This anti-correlation between MS and BSi records is in line with expectations, as increased biogenic input dilutes the terrigenous magnetic component of the sediment (Pudsey and Howe, 1998; Collins et al., 2012; Xiao et al., 2016). High maximum values of MS are recorded at 722 cmbsf, 455 cmbsf and 291 cmbsf (Suppl. Fig. S1). The MS record is mainly used for age model reconstruction (see Suppl. Inf.) and will not be further discussed here.

4.2. Ice-rafted debris

Ice-Rafted Debris (IRD) is present throughout the core (Fig. 2). High abundances of IRD (up to 135 clasts/10 cc) occur at 225, 383, 404, 499, 519, 584 and 743 cmbsf (~83, 140, 152, 213, 226, 265, and 360 ka, respectively). Peaks in the largest relative grain size (more than 5% of the IRD is larger than 2 mm) are located at 193, 233, 278, 395, 546 and 654 cmbsf (~70, 86, 103, 147, 242, and 307 ka, respectively). In general, the amount of IRD per 10 cc of sediment is higher during the glacial periods.

4.3. XRF: biogenic barium (Ba_{bio}) and elemental ratios

Ba_{bio} concentrations were never below 230 ppm. Ba_{bio} shows no significant correlation with elemental ratios most sensitive to detrital input (Zr/Rb) or redox conditions (V/Cr, Ni/Co, U/Th) (Suppl. Fig. S13). Therefore, this proxy is a reliable indicator of biogenic production. The elemental ratios for bottom water oxygenation V/Cr, Ni/Co and U/Th are generally within the oxic field defined by Jones and Manning (1994) (respectively below 2.0, 5.0 and 0.75, Suppl. Fig S13)). However, the V/Cr and U/Th values occasionally cross the oxic-dysoxic threshold, suggesting dysoxic bottom-water conditions around 96, 112, 138, 244 and 337 ka (Fig. 3). Ni/Co never shows values above the oxic-dysoxic threshold as defined by ones and Manning (1994) (Suppl. Fig. S13). Within these intervals where V/Cr and U/Th ratios suggest dysoxic bottom-waters, Ba_{bio} might be reduced due to post-depositional remobilization (McManus et al., 1998).

The reliability of Ba_{bio} as a proxy for paleoproductivity is confirmed by the resemblance of the Ba_{bio} record to the BSi record,

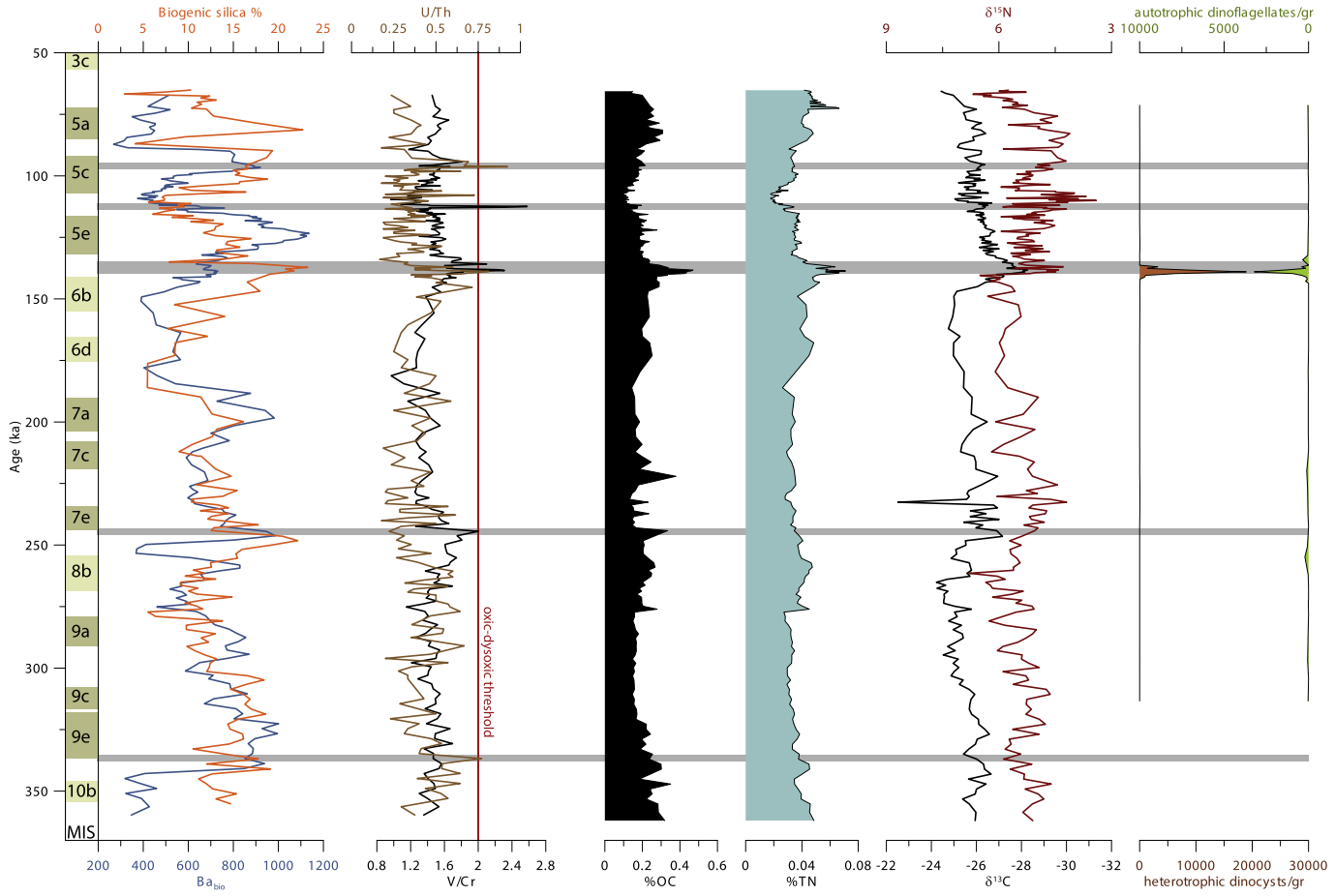

Fig. 3. Geochemical elements, biogenic silica organic carbon and nitrogen data obtained from core AS05-10. The dark red shading marks periods of dysoxic bottom-water conditions. The blue shading marks the position of the Terminations (as in Fig. 2). (For interpretation of the references to color in this figure legend, the reader is referred to the Web version of this article.)

especially in the lower part of the core (Fig. 3). The tight link between Ba_{bio} and BSi has been used for reconstructing paleoproductivity at other Southern Ocean sites, with increased Ba_{bio} and BSi values during interglacials south of the PF (Bonn et al., 1998; Pudsey and Howe, 1998; Hillenbrand and Fütterer, 2001; Hillenbrand et al., 2003, 2009). Interestingly, our record shows that the timing of each Ba_{bio} peak lags that of the BSi around the onset of each interglacial (MIS 9e, 7e, 7a-c and 5e, Fig. 3). The largest lag can be observed around the onset of MIS5e.

4.4. Biogenic silica

Biogenic silica (BSi) weight percentages vary between 4% and 23%. Maxima are recorded during Terminations (Fig. 3). Highest values are recorded during T-III (~248 ka) and T-II (~137 ka), but also during MIS5c (~90–100 ka) and MIS5a (~81 ka).

4.5. Organic carbon and nitrogen content and isotopes

Trends in weight percent organic carbon (%OC) and total nitrogen (%TN) are very comparable and show highest percentages at the onset of each interglacial stage. Peak values in both %OC and % TN coincide with maxima in BSi and/or Ba_{bio} (Fig. 3).

$\delta^{15}N$ values range between 3.4 and 6.8‰. Minima in $\delta^{15}N$ generally coincide with the onset of each major interglacial stage (MIS9e, MIS7e, MIS7a-c, MIS5e). Apart from those, three additional minima can be recognized at the onsets of MIS9c (~310 ka), MIS5c (~110 ka), and MIS5a (~90 ka), respectively.

The intercept with the y-axis of the linear regression line of the %OC versus %TN plot lies at 0.013 %TN (Suppl. Fig. S14), indicating no significant influence on the $\delta^{15}N$ value due to the presence of inorganic nitrogen or due to terrestrial input.

Branched versus isoprenoid GDGTs and TEX_{86}-based subsurface temperatures.

Maximum iGDGT concentrations around 140 ka (between 375 and 380 cmbsf) co-occur with maximum %OC values (Fig. 3; Fig. 4B). As abundances of branched GDGTs (brGDGTs) are relatively constant throughout the record, iGDGT concentrations determine the BIT index. The BIT shows a strong minimum of around 140 ka, otherwise being generally above 0.3 (Fig. 4B). The ternary diagram (Fig. 4A) shows that brGDGT compositions are very similar to those found on the Svalbard shelf (De Jonge et al., 2014; Sinninghe Damsté, 2016; Naafs et al., 2017; Dearing Crampton-Flood et al., 2019). In addition, the relative abundance of 6-methyl hexamethylated brGDGTs is high (between 56% and 94% of the total hexamethylated brGDGTs), which has been suggested to represent an adaptation to environments with a higher pH (i.e. sea water) (De Jonge et al., 2014), although such high relative abundances of 6-methyl brGDGTs are not commonly observed in a marine setting (values generally below 70%) (Sinninghe Damsté, 2016).

The composition of brGDGTs suggests that all brGDGTs are produced either *in situ* or have been transported from the Ross Sea shelf and are not derived from Antarctic soils. This was not unexpected, as soil production in glacial settings is low (Peterse et al.,

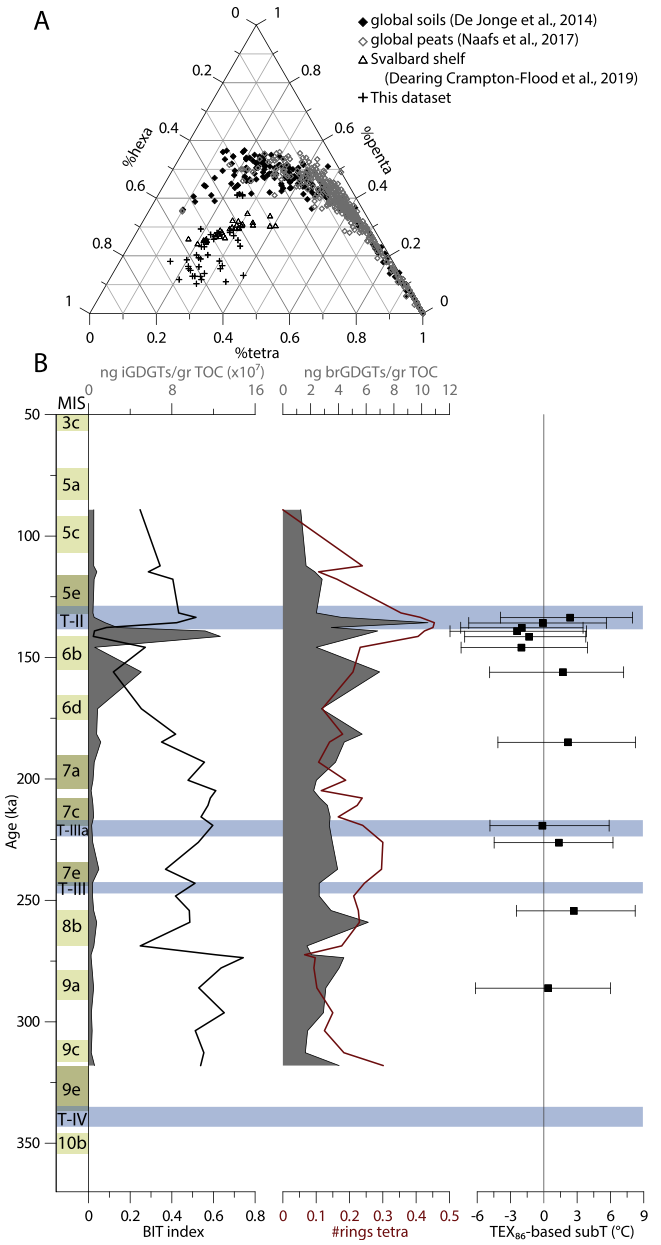

Fig. 4. A) Ternary diagram of the relative abundances of tetra-, penta-, and hexamethylated brGDGTs in samples obtained from core AS05-10 compared to global soils and peats, and sediments obtained from the Svalbard shelf. B) iGDGT and brGDGT data and a TEX86-based subsurface temperature reconstruction obtained from core AS05-10. Error bars of the subsurface temperature reconstruction show the width of the 10%-confidence interval according to the BAYSPAR calibration method. The blue shading marks the position of the Terminations (as in Fig. 2). (For interpretation of the references to color in this figure legend, the reader is referred to the Web version of this article.)

2009). Nevertheless, our record shows $\#rings_{tetra}$ values increasing and decreasing during interglacial and glacial periods, respectively (Fig. 4).

Only 12 of 38 samples selected contained sufficient iGDGTs to calculate a reliable TEX_{86} value. Most of these samples lie between 170 and 130 ka. The iGDGT data shows no indications of input from methanogenic or methanotrophic archaea (GDGT-0/Cren < 2 following Blaga et al. (2009), GDGT-2/Cren < 0.4 following Weijers et al. (2011), and MI < 0.5 following Zhang et al. (2011)) or other non-temperature related biases (|ΔRI| < 0.6 following (Zhang et al., 2016)) (see Suppl. Table S1). Because all brGDGTs are produced *in situ*, no samples have been discarded, because of high BIT values. TEX_{86} values range between 0.34 and 0.44. When converted to subsurface temperatures using the BAYSPAR calibration, temperatures vary between −2.4 °C and 2.7 °C with a 90%-confidence interval of ±5.8 °C (Fig. 4). Notably, our temperature reconstruction shows a minimum prior to Termination II and an increase towards the onset of MIS5e. Considering the much higher concentrations of iGDGTs in this interval compared to the rest of the record, these reconstructed temperatures are most reliable and most likely reflect subsurface warming at the onset of MIS5e.

4.6. Palynology

Only trace amounts of palynomorphs have been found: 34 out of 49 samples contain less than a 1000 palynomorphs per gram sediment. Four samples were completely barren. The *in situ* protoperidinioid dinoflagellate cysts in our samples include *Cryodinium meridianum*, *Nucicla umbiliphora* (Hartman et al., 2018b), *Selenopemphix antarctica* and *Selenopemphix* sp. *1* sensu Esper and Zonneveld (2007). *In situ* gonyaulacoids include *Impagidinium aculeatum*, *I. pallidum* and *I. variaseptum*. Generally, increased amounts of *in situ* palynomorphs co-occur with increased %OC (see Fig. 5). Notably, there is one prominent peak of dinoflagellate cyst (dinocyst) abundance between 143 and 134 ka (preceding the onset of MIS5e), coinciding with maximum %OC. Between 141 and 137 ka this peak is dominated by protoperidinioid (heterotrophic) dinocyst species: mainly *Selenopemphix antarctica* and *Cryodinium meridianum*. Apart from these protoperidinioids, also increased gonyaulacoid (mainly *Impagidinium pallidum*) and gymnodinioid (*Gymnodinium* spp.) dinoflagellate cysts are found in this interval, however in much lower absolute abundances (Figs. 5 and 7). Peak abundances of *I. pallidum* are also present downcore, in particular around 255 ka. Abundances of protoperidinioid dinocysts remain below 100 specimens/gram outside the 143–134 ka interval. Intervals with high abundances of the autotrophic species *I. pallidum* also show increased absolute abundances of *Leiosphaeridia* spp. and the prasinophyte *Cymatiosphaera* spp. (Fig. 5). Furthermore, several intervals with increased abundances of reworked Paleogene dinoflagellate cysts occur (*Vozzhenikova apertura* and *Spinidinium macmurdoense* (Bijl et al., 2013)), as well as Paleogene pollen and spores. Generally, these high abundances of reworked material precede the peaks of *I. pallidum*, *Cymatiosphaera* spp. and *Leiosphaeridia* spp.

4.7. Benthic foraminifers

Low numbers of agglutinated foraminifer species have been found in parts of the record associated with interglacial deposition. Most dominant species are *E. bradyi* and *M. nodulosa*. *E. bradyi* shows highest values during MIS5e. *M. nodulosa* is most abundant in the interval before MIS5e (Termination II). In comparison to *E. bradyi*, *M. nodulosa* is also more abundant during MIS7 (Fig. 5).

4.8. Diatoms

Absolute diatom valve counts show peak values at 137 and 245 ka, coeval with highest percentages of biogenic silica during Termination III and II (Fig. 6). Just prior to Termination IIIa diatom counts also peak, but there is no diatom data available for the period that encompasses Termination IIIa and interglacial 7a-c. Instead, diatom counts during Termination IV are relatively low, while BSi percentages are relatively high. Diatom valve counts only reach higher abundances during MIS9c and MIS9a. Diatom assemblages are dominated by alternating *Eucampia antarctica* and

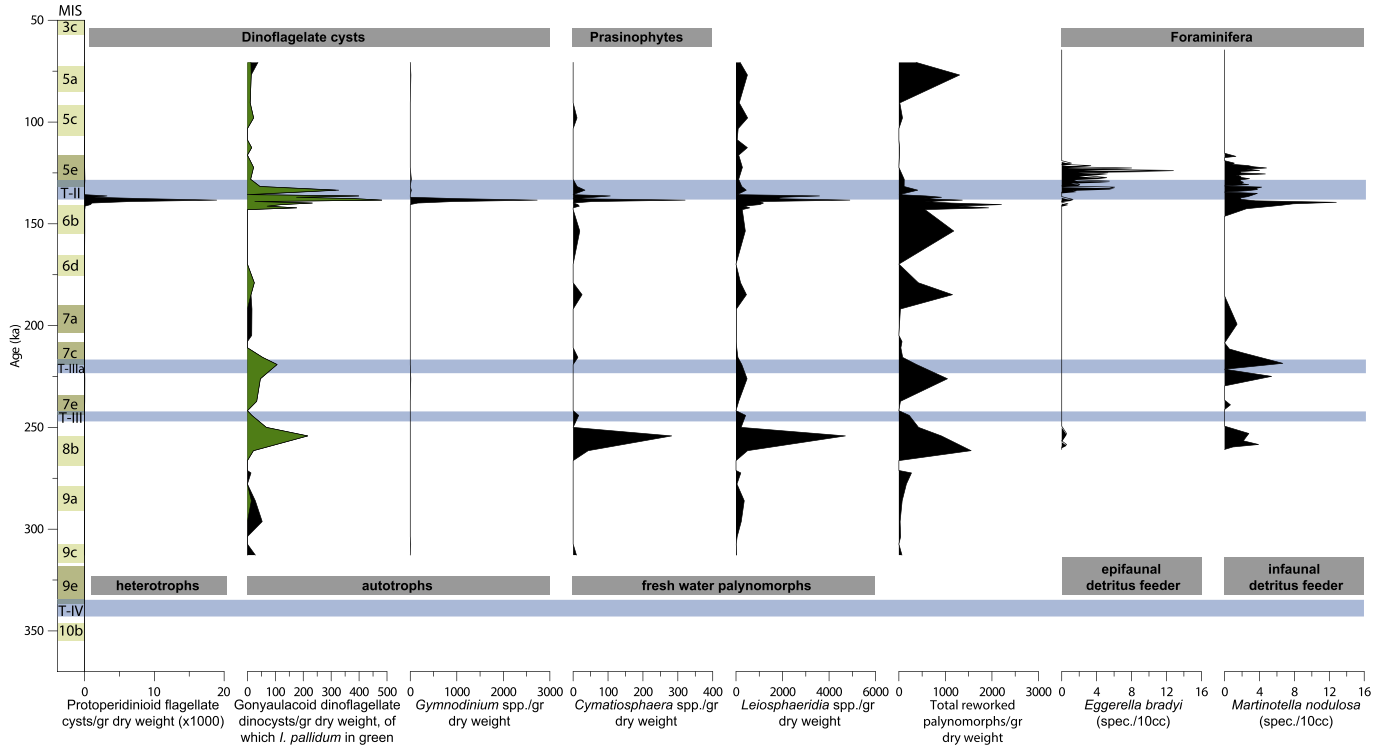

Fig. 5. Palynological and foraminifer data obtained from core AS05-10. The blue shading marks the position of the Terminations (as in Fig. 2). (For interpretation of the references to color in this figure legend, the reader is referred to the Web version of this article.)

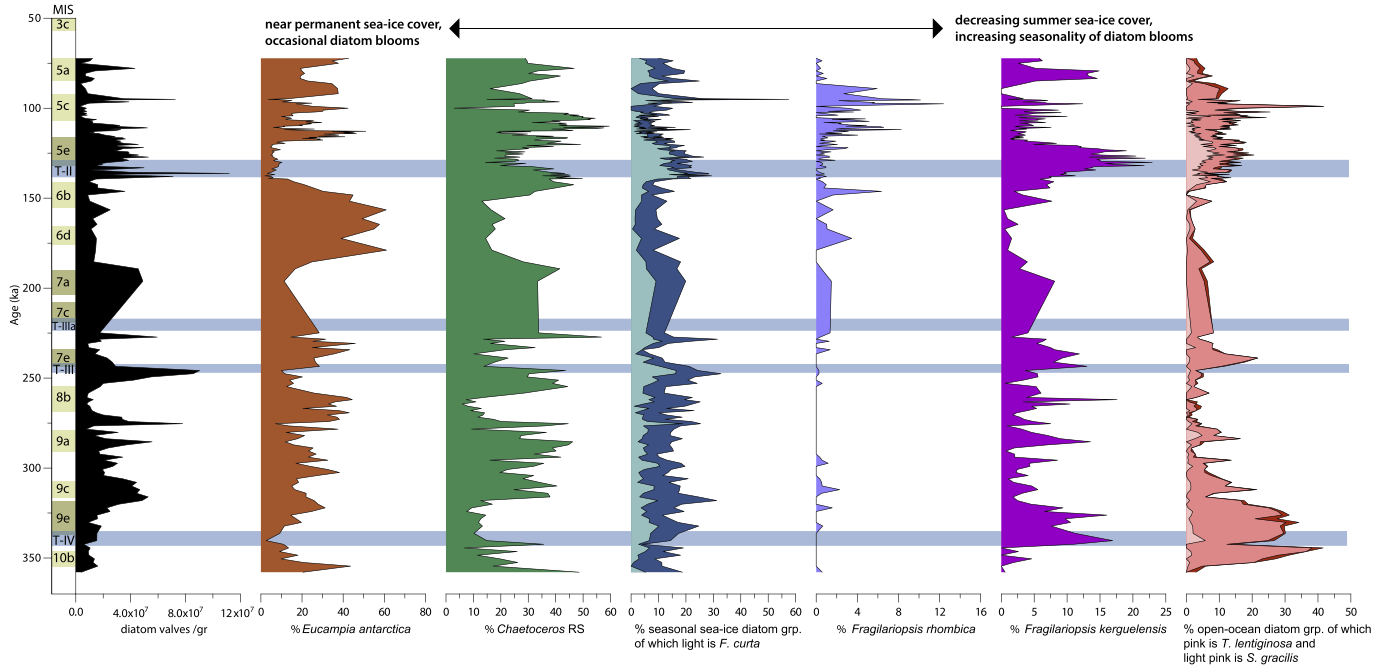

Fig. 6. The relative abundances of diatoms obtained from core AS05-10. The blue shading marks the position of the Terminations (as in Fig. 2). (For interpretation of the references to color in this figure legend, the reader is referred to the Web version of this article.)

Chaetoceros resting spores (RS) (Fig. 6).

In core AS05-10 the highest abundances of *E. antarctica* are typically associated with the glacials, when also diatom abundance is low. Of the two varieties of *E. antarctica* only *E. antarctica* var. *recta* were found and no specimens of *E. antarctica* var. *antarctica*. *E. antarctica* in our paper thus refers to var. *recta*. *%E. antarctica* during MIS8 are lower than during MIS6, and the onset and termination of glacial MIS8 are also less pronounced in comparison to MIS6. Following the high *%E. antarctica* during the glacials, each glacial-interglacial transition is characterized by a clear sequence of

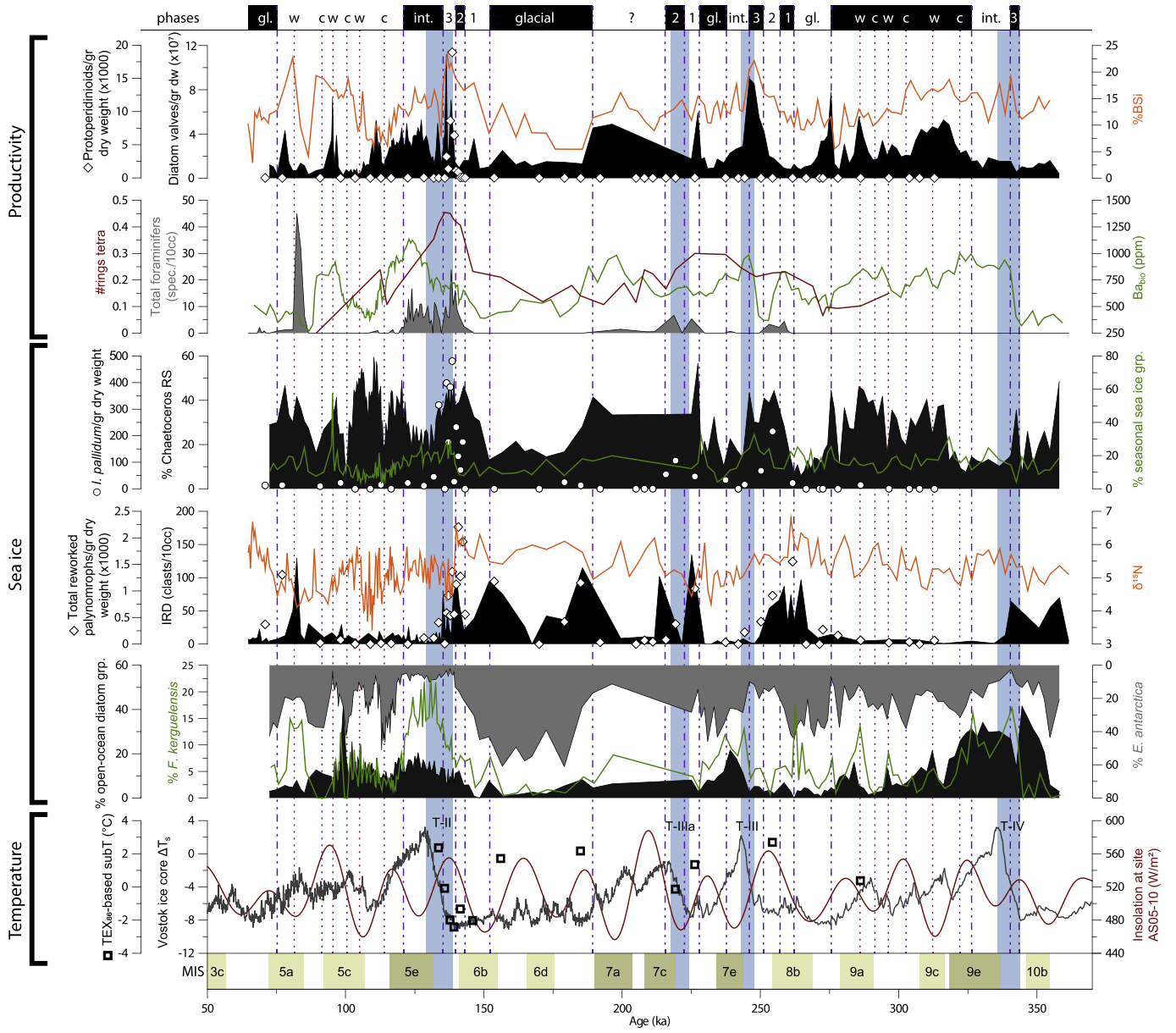

Fig. 7. The proxies that are indicative of temperature, sea ice and productivity combined and related to the air temperature record of the Vostok ice core and local insolation. The blue shading marks the position of the Terminations (as in Fig. 2). The phases of each glacial (gl.) - interglacial (int.) transitions (see text) are indicated at the top of the figure. Dotted vertical lines correspond to warm (w) and cold (c) oscillations of the glacial inception following interglacial conditions. (For interpretation of the references to color in this figure legend, the reader is referred to the Web version of this article.)

increased relative abundances of individual diatom species (Fig. 6): reduction of *%E. antarctica,* an increase in *%Chaetoceros* RS, increase of %seasonal sea-ice diatom group, and finally increased *%Fragilariopsis kerguelensis* and *%Thalassiosira lentiginosa*. In general, this sequence of diatom species abundances is reversed when transitioning from an interglacial to a glacial state.

%Chaetoceros RS are always higher than 10%, but generally highest during and preceding maxima of diatom valve counts (Fig. 6). These peak values precede each glacial-interglacial transition, where declining *%E. antarctica* are replaced by a dominance of *Chaetoceros* RS, rising above 40%. After or coincident with the increase in *%Chaetoceros* RS preceding each interglacial, the seasonal sea-ice diatom group reaches values of 20% or higher (Fig. 6). Still *Chaetoceros* RS make up the largest part of the diatom assemblage. Notably, maxima in the seasonal sea-ice diatom group are coeval with maxima in the absolute diatom abundance and its overall trend is dominated by the changes in *%Fragilariopsis curta*, especially during T-II and T-III.

Following peak *%F. curta*, the *%Fragilariopsis kerguelensis* (>10%) rises to a maximum together with or followed by the open-ocean group (>15%) during each interglacial. Although the open-ocean diatom group follows the distribution pattern of *F. kerguelensis* during MIS5e, they peak after *F. kerguelensis* during MIS9e and MIS7e. This group mainly consists of *Thalassiosira lentiginosa*. Notably, there are also increased *% Shionodiscus gracilis* during MIS5e, while it is generally very low in abundance in the rest of the record.

The glacial inception following each interglacial is characterized by increased *%Fragilariopsis rhombica*. Particularly high abundances occur during MIS5d and MIS5c. Minor peak abundances occur

during the glacial stages.

5. Discussion

5.1. Glacial-interglacial sea-ice variability and primary productivity

5.1.1. Glacial phases

The low diatom valve abundances in combination with high relative abundance of *Eucampia antarctica* during glacial periods at site AS05-10 (Figs. 6 and 7), especially MIS6, is consistent with other Southern Ocean records (Kaczmarska et al., 1993; Xiao et al., 2016). *E. antarctica* percentages in our record exceed those found in surface sediment samples south of the winter sea ice edge (WSE) within the seasonal sea-ice zone (SSIZ) (2%) (Zielinski and Gersonde, 1997; Esper et al., 2010), and even those found in surface sediment samples at or south of the summer sea-ice edge (SSE) (5%) (Esper et al., 2010). The high abundances of *E. antarctica* characterize what we define as the glacial phase in core AS05-10 (see Fig. 7) and suggest that the site was nearly permanently covered by sea ice during this phase. In support of this are the relatively high and/or increasing $\delta^{15}N$ values during the glacial phases of MIS6 and MIS8 (and the onset of MIS4) that coincide with relatively low Ba_{bio} values and BSi percentages (Fig. 7). This suggests high nutrient utilization during periods of low export productivity, indicating the $\delta^{15}N$ record reflects decreased nutrient supply, during glacial periods. A similar relation between $\delta^{15}N$ and glacial-interglacials was recorded in other locations south of the PF and is interpreted as reduced vertical deep-water nutrient supply resulting from (surface-water) stratification (François et al., 1997; Studer et al., 2015). A reduced nutrient availability is also supported by the low amounts of diatom valves/gr deposited during the glacial stages.

The presence of *Chaetoceros* RS during glacial phases (Fig. 7) suggests that despite the presence of sea ice, diatoms occasionally bloomed in – likely stratified – rare open water conditions. Because *Chaetoceros* RS is characterized by high growth rates and high preservation potential (Crosta et al., 1997; Rembauville et al., 2015), occasional intense blooms would still allow the preservation of RS within the sediments resulting in *Chaetoceros* being the most abundant species after *E. antarctica* during the glacials. The relatively low Ba_{bio} values and BSi percentages are in accordance with rare open-water conditions that allow for primary productivity. Considering that Antarctic ice sheet reconstructions during the Last Glacial Maximum (LGM) suggest that the ice shelf edge was close to site AS05-10 (Denton and Hughes, 2002), such rare open-water conditions could be early-spring, ice-free areas that formed through spring warming and advection of sea ice from the ice shelf edge by katabatic winds or possibly polynya formation, which would allow for occasional diatom blooms of especially *E. antarctica* and *Chaetoceros*. Support for polynya formation near AS05-10 comes from a nearby sedimentary record of the LGM where the presence of the planktonic foraminifer *Neogloboquadrina pachyderma* has been interpreted as related to a polynya-driven environment (Bonaccorsi et al., 2007; Smith et al., 2010). Polynyas at the shelf edge may in general have been more frequent during glacial phases than today, due to the proximity of upwelling intermediate waters at the Antarctic slope and strong katabatic winds that are funneled along depressions in the nearby paleo-ice sheet surface (Smith et al., 2010). However, the data do not indicate a permanent and/or efficient polynya present over AS05-10, because the relative abundance of *Chaetoceros* RS and high $\delta^{15}N$ values do not support upwelling of deeper waters at AS05-10 during the glacials (Denis et al., 2009). Moreover, a diatom assemblage of an efficient latent-heat polynya would contain higher abundances of *F. curta* (Mezgec et al., 2017). We therefore interpret the *E. antarctica*/*Chaetoceros* RS dominated diatom assemblages as evidence for occasional wind-driven open-water conditions at the shelf edge in early spring (Fig. 8). The presence of generally high concentrations of IRD during the glacial phases (Fig. 7) supports a nearby ice shelf, although such high concentration could also be the result of the lower sediment accumulation rates during the glacials (Cofaigh et al., 2001).

The reconstructed low productivity during the glacial phases (MIS6 and MIS8 in Fig. 3) seems to disagree with the relatively high %OC and %TN found during the periods of glacial inception (MIS7a-b and MIS9a-d in Fig. 3). This could be the result of a closed sum

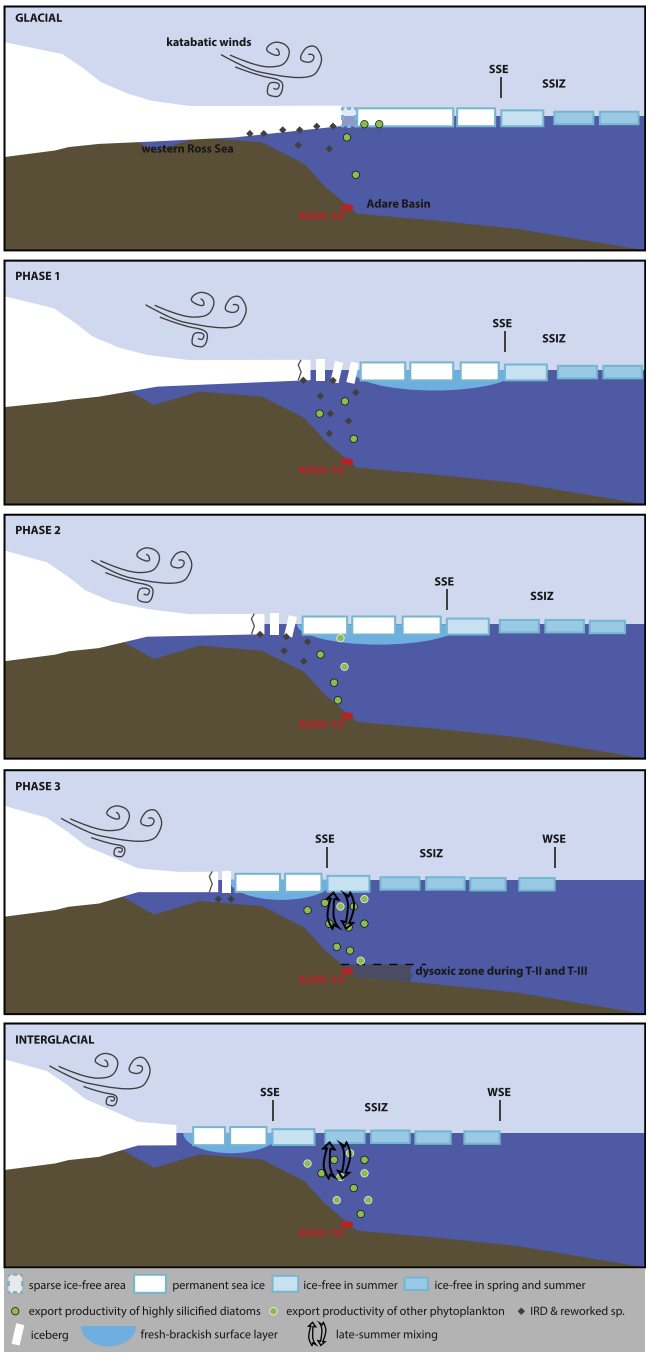

Fig. 8. An illustration the environmental conditions over site AS05-10 for the different phases of the glacial-interglacial transition described in the text based on the combined proxy records (see Fig. 7).

effect resulting from the decreased influx of biogenic and terrigenous siliciclastics during glacials. Alternatively, the transport of OC and TN to the seafloor might be enhanced during the glacial phase with respect to the period of glacial inception due to the short intense blooms and the effective transport of the heavy silicified diatom species *E. antarctica* and *Chaetoceros* RS, that dominate the glacial assemblages. *Chaetoceros* and *E. antarctica* RS have been shown to contribute substantially to the organic matter flux to the sea floor at other Southern Ocean sites (Salter et al., 2012; Rembauville et al., 2015, 2016). The relatively high OC and TN could also be originating from an increase of organic matter derived from reworked (non-marine) sediments from times when Antarctica was vegetated. Indeed, part of the reworked palynomorph assemblage consists of reworked pollen and spores, which represent up to 40% of the total palynomorph assemblage during glacials. However, as the intercept with the y-axis in the %OC versus %TN plot equals nearly 0 (Suppl. Fig. S14), a substantial influence of (non-marine) reworked organic matter can be excluded.

During the glacial, quite surprisingly, sufficient iGDGTs were found in the samples, which allowed to reconstruct water temperature based on TEX_{86} (Fig. 4). It is possible that during the glacials at site AS05-10, some of the occasional diatom blooms allowed for sufficient transportation of iGDGTs and their preservation within the sediments. Diatom blooms in general have been shown to contribute to the transportation and preservation of iGDGTs within surface sediments (Yamamoto et al., 2012; Schouten et al., 2013; Mollenhauer et al., 2015). Subsurface temperatures between −2 °C and 1 °C (with a 90%-confidence interval of ±5.8 °C) have been reconstructed for the glacial periods (Figs. 4 and 7). However, the highest temperatures are derived from sediments with low iGDGTs concentrations and may therefore be less reliable. The *E. antarctica* assemblage only consists of the symmetrical valves of the variety *recta*. As high relative amounts of symmetrical and terminal valves of *E. antarctica* var. *recta* versus asymmetrical and intercalary valves have been associated with SSTvalues below 0.5 °C (Allen, 2014), diatom findings support the TEX_{86}-based temperature reconstructions.

A comparison between the glacial phases of MIS8 and MIS6 shows that MIS8 has higher Ba_{bio} and %BSi and is characterized by relatively lower abundances of *E. antarctica* and higher abundances of *F. kerguelensis*, in agreement with other Southern Ocean diatom records (Kaczmarska et al., 1993; Xiao et al., 2016). This suggests that MIS8 may have been characterized by milder conditions in comparison to MIS6, allowing for more frequent open water, either through the retreat of the SSE to the glacial Ross Sea ice edge or through more efficient polynya activity (Mezgec et al., 2017). As a final remark, values for Ba_{bio}, %BSi and *%E. antarctica* during the glacial phase of MIS8 are very similar to those of MIS7d, also considered a glacial phase.

5.2. The glacial-interglacial transitions

We recognize three recurrent phases during each glacial-interglacial transition, representing a shift from dense sea-ice cover to seasonal sea ice: (1) ice-shelf break-up, (2) freshwater discharge and (3) the establishment of the MIZ over site AS05-10 (Figs. 7 and 8). The timing of these transitions coincides with air temperatures warming in the Vostok record of ~4 °C warming (Fig. 7).

Phase 1: the diatoms show a shift from an *E. antarctica*-dominated assemblage to an assemblage dominated by *Chaetoceros* RS, indicative of nutrient depleted waters (Leventer et al., 1996). Peaks in ice-rafted debris (IRD) and in the concentration of reworked dinoflagellate cysts during (but also just prior and after) this phase (Fig. 7), suggest ice shelf break-up and transport of sediments from the Antarctic shelf towards the coring site, possibly aided by iceberg rafting. In support, the reworked palynomorphs recovered from AS05-10 are of Eocene-Oligocene age. Sediments of this age are known to be exposed at the seafloor in the Ross Sea (Wilson et al., 1998; Hannah and Fielding, 2001). Furthermore, high concentrations of IRD and low diatom concentrations have been associated with ice-shelf break-up and associated iceberg release (Bentley et al., 2005; Minzoni et al., 2015). Peak $\delta^{15}N$ values during phase 1 (and phase 2 prior to MIS5e) also suggest higher nutrient utilization. Icebergs can supply iron and are known to fertilize the Southern Ocean (Duprat et al., 2016). As the growth of *Chaetoceros* RS is iron limited (Salter et al., 2012; Rembauville et al., 2015, 2016), stratified waters and iron fertilization through the break-up of the Ross Sea ice shelf would provide an ideal environment for *Chaetoceros* blooms, in line with our results (Fig. 8). Likely, increased stratification resulting from the increased input of freshwater due to the retreat of local glaciers and the associated break-off of large icebergs from ice shelves prohibits nutrient replenishment through vertical mixing. Enhanced nutrient utilization due to increased productivity is instead induced by a higher light penetration due to a decrease in sea ice cover. We interpret the combination of the proxy trends as an early warming signal. Although a direct relation with local insolation cannot be proven, phase 1 remarkably coincides with a period of increasing local insolation. Interestingly, this initial warming in our record precedes the atmospheric warming as recorded in the Vostok ice core, which could mean that ice shelf break-up was initiated by warming of the ocean waters. Although the Earth's climate is currently in a different state, the process of ice-shelf thinning and iceberg break-off due to basal warming occurs also today (Liu et al., 2015; Paolo et al., 2015) and results in an increased freshwater release, which seems to be promoting expansion of the sea-ice covered area around Antarctica (Bintanja et al., 2013).

Phase 2 is characterized by increasing fresh-, brackish water palynomorphs (*Cymatiosphaera* spp. and *Leiosphaeridia* spp.), while *Chaetoceros* RS reach peak abundances (Figs. 5 and 7). Although the taxonomic affinities of leiospheres are unknown, they have been associated with extensive presence of sea ice in paleoclimatic reconstructions (Wrenn et al., 1998; Troedson and Riding, 2002; Hartman et al., 2018a). High abundances are associated with a freshwater surface layer: the summer sea-ice margin and disintegrating pack ice during spring (Mudie, 1992; Mudie and Harland, 1996). Similarly, *Cymatiosphaera* spp. are typically associated with normal-to-low salinity and nutrient-rich surface waters and stratified waters (Mudie, 1992; Mudie et al., 2011) and have been interpreted as freshwater indicators in Antarctic paleoreconstructions (Wrenn et al., 1998; Hannah, 2006). During this second phase, the gonyaulacoid autotrophic dinoflagellate cyst *Impagidinium pallidum* increased its abundances (Fig. 7). *I. pallidum* has been found in surface sediments underlying recently collapsed ice shelves (Pieńkowski et al., 2013) and is known to withstand low-salinity waters (Zonneveld et al., 2013). This ecological niche may explain its absence during the interglacial phase, when longer open water conditions may favor other autotrophic dinoflagellates. Compared to phase 1, palynology and the relatively high amounts of *Chaetoceros* RS suggest the spring/summer melt and likely the retreat of the Ross Sea ice shelf results in a more frequent establishment of highly stratified fresh-brackish water lenses, promoting blooms of *Chaetoceros* and *I. pallidum* (Fig. 8). However, similar to phase 1, the relatively low abundance of seasonal sea-ice diatoms and the presence of IRD and reworked palynomorphs suggest that surface waters were still influenced by the presence of sea-ice and icebergs throughout most of the year. Such sea-ice coverage would have limited productivity, which is confirmed by low total diatom abundances (valves/g, Fig. 7). Periodical freshening of the surface

waters and stratification during phase 2 may have favored the formation of sea ice in the Ross Sea (Zhang, 2007). Notably, modern-day sea-ice concentrations in the Ross Sea show a non-linear, but on average increasing trend prior to 2014 (Comiso and Nishio, 2008; Parkinson, 2019), while the different water masses of the Ross Sea have also been freshening prior to 2014 (Castagno et al., 2019).

Phase 3: total diatom abundances (valves/g) and %BSi increase to a maximum during this phase (Fig. 7). *Chaetoceros* RS is still the dominant diatom species. *Chaetoceros* RS are heavily silicified and account for most of the high total diatoms in the sediment, being likely responsible for the peak in %BSi. During this phase, *Chaetoceros* RS is accompanied by peak abundances of the seasonal sea-ice diatom group, in particular *F. curta*. At present, this group appears during early spring when the sea ice is still present and dominates the surface waters during summer, particularly in the Marginal Ice Zone (MIZ) (Gersonde and Zielinski, 2000; Armand et al., 2005; Grigorov et al., 2014; Malinverno et al., 2016), the most productive ecological province of the Southern Ocean today (Fitch and Moore, 2007; Arrigo et al., 2008). *F. curta* and other seasonal sea-ice diatoms are small and they can easily float in stratified waters (Leventer, 1998). However, because of their small size, these seasonal sea-ice diatoms are very prone to dissolution (Grigorov et al., 2014), and only a high-productivity environment, like that of the MIZ, will favor their high occurrence in the sediment. The proximity of our site to the MIZ and therefore to the SSE during phase 3 is supported by the high total diatom abundance, %BSi and increasing Ba_{bio}. Today, the seasonal spring diatom blooms of the MIZ are suppressed by seasonal mixing of the surface waters during late summer due to increased winds (Arrigo et al., 1998; Fitch and Moore, 2007). Disruption of the pycnocline allows for the settling and preservation of these dissolution-susceptible diatom species (Denis et al., 2006). Increased mixing of deeper waters with the surface waters during this phase is reflected in the decrease in $\delta^{15}N$ values, which is particularly clear during the MIS6/MIS5 glacial-interglacial transition. The drop in $\delta^{15}N$ values suggests decreased nutrient utilization during this phase, and probably an increased nitrogen supply from mixing with deeper waters. In contrast to phase 2, the relatively low amounts of IRD during phase 3, suggest surface water stratification during phase 3 are much less the result of the retreat of the Ross Sea ice shelf. Instead, the presence of *F. curta* in combination with high total diatom abundances and low $\delta^{15}N$ values suggests ~ three months ice-free surface waters (Armand et al., 2005) and stratification due to the seasonal melt-back of sea ice in spring/summer, then disrupted by (late) summer mixing (Fig. 8).

For the glacial-interglacial transition related to Termination IIIa (the onset of MIS7c), we lack the diatom data to fully recognize all three phases of the transition. Phase 1 and 2 could be recognized based on high amounts of reworked palynomorphs together with IRD and high increased abundances of *I. pallidum*, respectively. Notably, Termination IIIa has been associated with ice-shelf break-up in the northern hemisphere as well, due to unusually high summer insolation following unusually low summer insolation at 65°N (Cheng et al., 2009).

Assuming we have recovered the full extent of the MIS10/MIS9 transition starting with the sharp drop in *E. antarctica* abundances around 355 ka, this glacial-interglacial transition differs in some respects from the MIS8/MIS7 and MIS6/MIS5 transitions. Surface water stratification appears to have been less intense/permanent prior to Termination IV (relatively low amounts of *Chaetoceros* RS and $\delta^{15}N$ values). Possibly, surface waters were already seasonally ice-free during MIS10 and/or meltwater release from the retreat of the ice shelf was less during this glacial-interglacial transition. Still increased IRD around 355 ka indicates ice-shelf break-up at that time, although the amounts are relatively low in comparison to the other glacial-interglacial transitions (Fig. 7).

During the MIS10/MIS9 transition, sea ice-free waters seem to have been reached very rapidly in spring, as *E. antarctica* is replaced by very high relative abundances of *T. lentiginosa*, which is a spring bloomer preferring low sea-ice concentrations (Crosta et al., 2005b; Esper et al., 2010). However, as *T. lentiginosa* produces large highly silicified valves (Shemesh et al., 1989), the record may be affected by preservation bias if silica dissolution or high bottom-water strength have removed the smaller (e.g., *Chaetoceros* RS, *E. antarctica*) and more dissolution-susceptible (e.g., *F. kerguelensis*, *F. curta*) diatom valves.

Both glacial-interglacial transitions related to Termination II (MIS6/MIS5) and III (MIS8/MIS7) show signs of oxygen-depleted bottom-water conditions (high V/Cr ratios, high %OC and high % TN; Fig. 3) in association with increased surface-water PP. But several differences between the MIS6/MIS5 and MIS8/MIS7 transitions suggest that bottom-water conditions at the onset of Termination II were more oxygen-depleted (Fig. 7):

1) %BSi starts increasing during phase 1 comparably, reaching a maximum during phase 3, while Ba_{bio} shows a different trend, with a plateau during phase 3 of the MIS6/MIS5 transition, while rising sharply during phase 3 of the MIS8/MIS7 transition. Low oxygen conditions can result in post-depositional remobilization of barium (McManus et al., 1998).
2) Only phase 3 of the MIS6/MIS5 transition shows a peak in the concentration of heterotrophic protoperidinioid cysts. Protoperidinioid cysts are sensitive to oxic degradation (Versteegh and Zonneveld, 2002; Reichart and Brinkhuis, 2003), which also explains their absence in most of the record, while they typically dominate Southern Ocean surface sediments south of the PF (Esper and Zonneveld, 2002; Zonneveld et al., 2013).
3) BIT values show a decrease, reaching minimum values, during the transition phases preceding Termination II and not during the transition phases preceding Termination III. iGDGTs degrade more easily than brGDGTs (which, in our record, are exclusively marine-produced) in oxygen-rich environments (Huguet et al., 2008, 2009). Increasing iGDGT concentrations preceding Termination II, while concentrations of brGDGTs show little change (Fig. 4), therefore suggest increased organic matter preservation.

The abundant presence of iGDGTs during the second and third phase of the MIS6/MIS5 transition allows for the reconstruction of subsurface (0–200 m) temperatures (subT) based on TEX_{86}. Temperature increases from −2.4 to 2.3 (with a 90%-confidence interval of ±5.8 °C) (Figs. 4 and 7). GDGTs are here interpreted to represent a spring/summer temperature signal, because archaeal communities bloom in spring after the sea-ice retreat (Murray et al., 1998; Church et al., 2003). Furthermore, GDGTs acquire pelleting to sink effectively to the sea floor (Schouten et al., 2013), and highest sedimentary GDGT fluxes are closely linked to highest organic matter, opal (diatom frustules) and lithogenic particle fluxes during the spring/summer season (Yamamoto et al., 2012; Mollenhauer et al., 2015). Today the difference between the summer SST and the 0–200 m depth-integrated temperature is 2 °C. Assuming this difference has remained constant, reconstructed summer SSTs rose from −0.4 to 4.3 °C during Termination II. The high abundances of *F. curta* and *Chaetoceros* RS in this interval would suggest sea surface temperatures between −1.5 and 1 °C (Armand et al., 2005), in agreement with reconstructed TEX_{86}-based temperatures. The reconstructed (sub-)surface temperatures preceding peak warmth of MIS5e are 2.5 °C warmer than (sub-)surface temperatures today (Locarnini et al., 2010). The few temperature estimates around the

time of the MIS8/MIS7 transition show similar subsurface temperature estimates as those reconstructed for the MIS6/MIS5 transition (between 0 and 2 °C with a 90%-confidence interval of ±5.8 °C), although these subTs are based on much lower iGDGT concentrations and could therefore be less reliable.

5.3. Interglacial phase

Maximum atmospheric temperatures over Vostok during peak interglacials coincide with decreasing seasonal sea-ice diatom abundances and a sharp rise in *F. kerguelensis* (although never > 25%), and subsequently an increase in open-ocean diatoms (mainly *T. lentiginosa*) (glacial phase in Fig. 7). The transition from relatively more *F. curta* to relatively more *F. kerguelensis* within the diatom assemblage marks the transition to a surface-water environment that more frequently experiences a longer sea ice-free season and summer SSTs above 1 °C (Armand et al., 2005; Crosta et al., 2005a, 2007). Considering that *F. kerguelensis* and *T. lentiginosa* are early bloomers with respect to *F. curta* and other seasonal sea-ice diatoms (Grigorov et al., 2014), their increased abundances seem to reflect an advancement of the spring/summer melt and a prolongation of the blooming season. Increased annual PP is further supported by peak Ba_{bio} values, indicating increased export productivity. The longer blooming season and therefore increased export productivity of biogenic silica to the seafloor has attributed to the increased sedimentation rates during the interglacial phases with respect to the glacial phases, particularly for MIS5e (see Supplementary Information). For comparison, the depth interval containing 50 kyr of MIS6 is 60 cm, while the depth interval containing 10 kyr of MIS5e is 75 cm. However, this is not reflected in the height of %BSi or the diatom counts per gram, probably because of the simultaneous increase in detrital flux. Alternatively, other non-siliceous plankton species than diatoms have contributed to the maximum export productivity during the interglacial phase.

The high abundances of *F. kerguelensis,* which dominates the region north of the SSE today (Esper et al., 2010), reflect a more southward position of the SSE during MIS9e, MIS7e and MIS5e (no data for MIS7a-c available). The increase of *T. lentiginosa* during MIS9e, MIS7e and MIS5e (often coincident with a decrease in *F. kerguelensis*) could represent an even further reduction of annual sea-ice cover and proximity of the WSE (Crosta et al., 2005a; Esper et al., 2010). Still, *Chaetoceros* RS and the seasonal sea-ice diatoms account for at least 40% of the total diatom assemblage, suggesting that the surface waters overlying Site AS05-10 are still affected by the seasonal melt and lie within the SSIZ (Fig. 8).

Comparing the various interglacial phases, highest abundances of *F. kerguelensis* are found during MIS5e, suggesting this interglacial phase experienced furthest-reduced sea-ice cover, most-frequently reduced sea-ice cover, or both. However, a notable difference of MIS5e with the other interglacials is that a larger fraction of the open-ocean diatom group is composed of *S. gracilis* (Fig. 6). Although *S. gracilis* is an early bloomer like *F. kerguelensis* and *T. lentiginosa* (Grigorov et al., 2014), it is associated with cooler summer SSTs (Crosta et al., 2005a; Esper et al., 2010). This would suggest that SSTs during MIS5e might have been cooler than during MIS9e and MIS7e, which is in contrast to deuterium-based air temperature reconstructions from the Vostok ice core (Petit et al., 1999). However, in contrast to *T. lentiginosa*, both *S. gracilis* and *F. kerguelensis* also bloom later during summer (Grigorov et al., 2014). Therefore, a more likely scenario would be that MIS5e experienced a longer blooming season due to more open waters in late summer, which allowed for the production and preservation of relatively more *S. gracilis* and *F. kerguelensis* versus *T. lentiginosa*.

Alternatively, shifts in relative abundances between the seasonal sea-ice diatoms, *F. kerguelensis* and the open-ocean diatoms *T. lentiginosa* and *S. gracilis* can be caused by differences in the susceptibility of these diatoms to dissolution. In general, however, the constant presence of dissolution-susceptible diatoms like *F. curta* and other seasonal sea-ice diatoms suggests that large changes in silica dissolution have not significant influenced the record of site AS05-10.

The relatively high abundances of *F. kerguelensis, S. gracilis* and *T. lentiginosa* during MIS5e would suggest summer SSTs of at least 1 °C (Crosta et al., 2005a; Esper et al., 2010). Although we have no TEX_{86}-based temperature reconstruction during the peak interglacial period, surface temperatures were possibly at or higher than the ~4 °C reconstructed for Termination II. A recent compilation of several (summer) sea surface temperatures of the Southern Ocean for MIS5e, based on various proxies, shows estimates for the modern-day Antarctic Zone (50–60°S) between 3.1 and 6.1 °C (Chadwick et al., 2020). One diatom-based temperature estimate from the SSIZ in the Weddell Sea (58.72°S) lies around 1.3 °C (Bianchi and Gersonde, 2002; Chadwick et al., 2020). Considering the latitudinal position of site AS05-10 (70.835°S), our TEX_{86}-based temperature estimate for MIS5e appears therefore relatively high. However, our TEX_{86}-based temperature difference of 2.5 °C warmer than today is supported by other polar estimates (McKay et al., 2011), which are higher than the 0.7 °C global average difference (McKay et al., 2011), in part due to the effect of polar amplification. Together with other estimates, our results would contradict the conclusions by Serreze and Barry (2011) who suggested no Antarctic polar amplification in the near future, because surface waters around Antarctica probably remain cold enough to support sea ice, due to the presence of the Antarctic ice sheet and the cold katabatic outflow of surface winds over the coastal waters. In the Ross Sea, katabatic winds are particularly strong during winter (Nylen et al., 2004), where they control the ongoing formation of sea ice in Terra Nova Bay (Bromwich and Kurtz, 1984; Jacobs et al., 1985; Budillon et al., 1999). Although our diatom data also support sea ice during the winter, the summer temperatures are higher than at present. Seasonality seems to have increased during the last interglacial, and may therefore also increase due to future warming.

5.4. The glacial inception

In line with the study of the Past Interglacials Working Group of PAGES (2016), we have termed the period following an interglacial "the glacial inception". Focusing on MIS5, the glacial inception following MIS5e is characterized by relatively lower PP and increased sea-ice concentrations, as indicated by the increased abundances of *Chaetoceros* RS, lower abundances of *F. kerguelensis*, and generally lower BSi and Ba_{bio} values (Figs. 6 and 7). During MIS5a-d, warm and cold periods can be inferred by the changes in abundance of the various diatom species, Ba_{bio} and %BSi. Peak Ba_{bio} and BSi values, high relative abundances of *F. kerguelensis* and open-ocean diatoms, and relative abundances of *E. antarctica* reaching a minimum, characterize the warmest phases, while the coldest phases are characterized by the opposite (red and blue dotted vertical lines in Fig. 7). The cold and warm phases correspond to stadials (MIS5b and d) and interstadials (MIS5a and c) in the Vostok ice core record. However, low relative abundances of *E. antarctica* and relatively high abundance of seasonal sea-ice diatoms suggest an additional warm/sea ice reduced phase during the late part of MIS5c, which coincides with peak solar insolation. Notably, peak local insolation at site AS05-10 during MIS5c also coincides with the highest abundances of *F. rhombica* (Figs. 6 and 7), a species that has been associated with relatively warm surface waters and/or low sea-ice concentrations compared to other sea-ice diatoms (Denis et al., 2006; Crosta et al., 2007, 2008).

Although the data resolution is lower, a similar pattern of cold and warm oscillations can be observed for MIS9a-d.

5.5. Productivity at the sediment surface

Productivity at the sediment surface seems to be tightly linked to productivity in the surface waters. Increased abundances of the benthic foraminifer species *Martinottiella nodulosa* and *Eggerella bradyi* occur during the period of highest PP, MIS5e (Figs. 5 and 7). Peak abundances of benthic foraminifers, particularly *M. nodulosa*, just prior to MIS5e show strong correlation with the IRD record and the abundance of reworked palynomorphs (prior to Termination III, IIIa and II), thus suggesting these peak abundances are caused by local reworking.

A dominant association of *Eggerella* and *Martinottiella*, but in low amounts, is generally associated with a depositional environment below the calcite compensation depth (CCD) as they have high preservation potential (Mackensen et al., 1990; Harloff and Mackensen, 1997). Currently, a very diverse agglutinated benthic foraminifer assemblage dominates the calcareous benthic foraminifer assemblage in the western Ross Sea (Asioli, 1995). Furthermore, calcareous planktonic foraminifera are common in the western Ross Sea in the surface waters (Asioli and Langone, 1997; Bergami et al., 2009 and references therin). The absence in the AS05-10 record of both planktic and benthic calcareous foraminifer species, as well as the lack of a diverse agglutinated benthic foraminifer assemblage, of which most use some form of calcite to glue their tests, seems to suggest carbonate dissolution by corrosive bottom-waters.

In response to increased surface water productivity, sedimentary archaeal productivity was likely also promoted. Indeed, highest brGDGT concentrations are recorded during peak diatom export productivity during Termination II (Fig. 4). Increased archaeal productivity is, however, mostly reflected in the $\#rings_{tetra}$ (Figs. 4 and 7). Because input of soil-derived brGDGTs can be expected to be very low in glacial settings (Peterse et al., 2009) and dust-blown soil-derived brGDGTs have been shown to be of minor contribution to distal marine settings (Weijers et al., 2014), the input on acyclic brGDGTs must be very low. Therefore, the recorded trends of increased $\#rings_{tetra}$ during the interglacials and decreased $\#rings_{tetra}$ during the glacials must simply reflect increased input of marine brGDGTs at Site AS05-10. Alternatively, these marine brGDGTs were transported from the Ross Sea shelf to Site AS05-10.

6. Conclusions and implications for future warming

Core AS05-10 retrieved from the slope between the Drygalski basin and the Adare Basin records the response of the surface water environment to glacial-interglacial variability in the late Pleistocene. Our multiproxy study identified three phases in each glacial-interglacial transition, which reflect the retreat of the seasonal sea-ice margin and warming of the surface waters.

Phase 1 is characterized by ice-shelf break-up and occasional ice-free areas. Phase 2 is characterized by meltwater runoff resulting in highly stratified waters. The progressive warming caused a retreat of the summer sea-ice edge, and brought the marginal sea-ice zone over site AS05-10 during Phase 3. During this phase the surface waters were seasonally stratified, instead of permanently stratified like during glacials, allowing for the replenishment of nutrients from the deep water through vertical mixing. Following the glacial-interglacial transition, an increased duration of ice-free conditions during the interglacials allowed open-water diatoms to proliferate. Increased (export) productivity during the interglacials is also reflected in the increased abundances of benthic agglutinated foraminifers and branched GDGTs. The highest productivity was reached during MIS5e due to an increased length of the blooming season and an increased supply of nutrients. TEX_{86}-based temperature values suggest summer temperatures of 2.5 °C warmer than today during MIS5e.

Our record clearly reflects the migration of the highly productive marginal ice zone to higher latitudes during interglacials. It is therefore clear evidence that the position of the summer sea ice edge and therefore the size of the marginal ice zone (MIZ) are influenced by past global warming phases. Future warming might shift the northern boundary of MIZ of the Ross Sea to even higher latitudes and could thereby reduce the size of this high-productivity zone (Sarmiento et al., 2004; Arrigo et al., 2008; Deppeler and Davidson, 2017).

Our record shows that warming is accompanied by an increased meltwater influx to the surface waters. Notably, the initial phases of ice-shelf break-up and surface water stratification precede the increase in air temperatures over Vostok and point to the fundamental role of the ocean on the cryosphere melting. It has been suggested that increased stratification could result in a shift from a *Phaeocystis*-dominated environment (like today) to a diatom-dominated environment, which could reduce the drawdown of CO_2 to the ocean floor (Arrigo et al., 1999; Steinacher et al., 2010; Vancoppenolle et al., 2013). We did reconstruct increased abundances of fresh-brackish water indicators *Leiosphaeridia* spp. and the prasinophyte *Cymatiosphaera* spp. in association with these highly stratified waters. Although initial conditions during current global warming are different from a glacial period, sea-ice cover in the Southern Ocean today is increasing due to increased meltwater runoff from the continent (Comiso and Nishio, 2008; Turner et al., 2009; Bintanja et al., 2013). If the melt phase at the onset of each glacial Termination in our record is equivalent to the increased freshwater release into the Southern Ocean today, we can expect sea-ice cover to decrease eventually in the Southern Ocean, like is happening in the Arctic already (Kay et al., 2011; Notz and Marotzke, 2012).

Author contribution

FS, AA, LL designed the project. JDH performed palynological and GDGT analyses, with the supervision of FS and PKB. MAB performed diatom analyses; AA performed foraminifer and IRD analyses, LL, FTa, FG, SA performed sedimentological and geochemical analyses. JDH wrote the paper with the input of all the other authors.

Data availability

All data are deposited in Zenodo (open access), https://doi.org/10.5281/zenodo.5032319 or can be asked at the corresponding author.

Declaration of competing interest

The authors declare that they have no known competing financial interests or personal relationships that could have appeared to influence the work reported in this paper.

Acknowledgements

Julian D. Hartman, Francesca Sangiorgi and Peter K. Bijl acknowledge the NWO Netherlands Polar Program project number 866.10.110. Diatom, foraminifera, IRD and geochemical (OC, $\delta^{15}N$, biogenic silica, XRF) analysis were performed within the frame of the PNRA 2009/A2.01 project "Sub-milankovian paleoclimatic variations and deep circulation linkages during the Late Quaternary

(MIS 5–7) in the Ross Sea slope (Antarctica)" (PI Alessandra Asioli). Maria Ángeles Bárcena acknowledges the Spanish projects CGL2015-68459-P and RTI2018-09489-B-100. We thank Dominika Kasjaniuk and Natasja Welters of the Utrecht University laboratory for their assistance in preparing the GDGT samples and palynological slides. We thank Francien Peterse and Stefan Schouten for the useful discussions on the interpretation of GDGT-based proxies.

Appendix A. Supplementary data

Supplementary data to this article can be found online at https://doi.org/10.1016/j.quascirev.2021.107069.

References

Abe, M., Nozawa, T., Ogura, T., Takata, K., 2016. Effect of retreating sea ice on Arctic cloud cover in simulated recent global warming. Atmos. Chem. Phys. 16, 14343–14356. https://doi.org/10.5194/acp-16-14343-2016.

Allen, C.S., 2014. Proxy development: a new facet of morphological diversity in the marine diatom *Eucampia antarctica* (Castracane) Mangin. J. Micropalaeontol. 33, 131–142.

Alley, K., Patacca, K., Pike, J., Dunbar, R., Leventer, A., 2018. Iceberg Alley, East antarctic margin: continuously laminated diatomaceous sediments rom the late Holocene. Mar. Micropaleontol. 140, 56–68. https://doi.org/10.1016/j.marmicro.2017.12.002.

Altabet, M.A., Francois, R., 2001. Nitrogen isotope biogeochemistry of the antarctic polar frontal zone at 170°W. Deep-Sea Res. Pt II 48, 4247–4273.

Altabet, M.A., Francois, R., 1994. Sedimentary nitrogen isotopic ratio as a recorder for surface ocean nitrate utilization. Global Biogeochem. Cycles 8, 103–116.

Andry, O., Bintanja, R., Hazeleger, W., 2017. Time-dependent variations in the Arctic's surface Albedo feedback and the link to seasonality in sea ice. J. Clim. 30, 393–410. https://doi.org/10.1175/JCLI-D-15-0849.1.

Armand, L.K., Crosta, X., Quéguiner, B., Mosseri, J., Garcia, N., 2008. Diatoms preserved in surface sediments of the northeastern Kerguelen Plateau. Deep-Sea Res. Pt II 55, 677–692. https://doi.org/10.1016/j.dsr2.2007.12.032.

Armand, L.K., Crosta, X., Romero, O., Pichon, J.J., 2005. The biogeography of major diatom taxa in Southern Ocean sediments: 1. Sea ice related species. Palaeogeogr. Palaeocl. 223, 93–126. https://doi.org/10.1016/j.palaeo.2005.02.015.

Arrigo, K.R., Dijken, G.L. Van, Bushinsky, S., 2008. Primary production in the Southern Ocean , 1997 – 2006. J. Geophys. Res. 113, C08004. https://doi.org/10.1029/2007JC004551.

Arrigo, K.R., Robinson, D.H., Worthen, D.L., Dunbar, R.B., DiTullio, G.R., VanWoert, M., Lizotte, M.P., 1999. Phytoplankton community structure and the drawdown of nutrients and CO2 in the Southern Ocean. Science 283, 365–367. https://doi.org/10.1126/science.283.5400.365.

Arrigo, K.R., Weiss, A.M., Smith, W.O.J., 1998. Physical forcing of phytoplankton dynamics in the southwestern Ross Sea. J. Geophys. Res. 103, 1007–1021.

Arrigo, K.R., Worthen, D.L., Robinson, D.H., 2003. A coupled ocean-ecosystem model of the Ross Sea: 2. Iron regulation of phytoplankton taxonomic variability and primary production. J. Geophys. Res.-Oceans 108, 3231. https://doi.org/10.1029/2001JC000856.

Arzel, O., Fichefet, T., Goosse, H., 2006. Sea ice evolution over the 20th and 21st centuries as simulated by current AOGCMs. Ocean Model. 12, 401–415. https://doi.org/10.1016/j.ocemod.2005.08.002.

Asioli, A., 1995. Living (stained) benthic foraminifera distribution in the western Ross Sea (Antarctica). Palaeopelagos 5, 201–214.

Asioli, A., Langone, L., 2010. "Living" (CTG vs rose Bengal) benthic foraminifera distribution in western Ross Sea (Antarctica). In: International Symposium on Foraminifera. FORAMS 2010 Abstracts, p. 51.

Asioli, A., Langone, L., 1997. Relationship between recent planktic foraminifera and water mass properties in the Wester Ross Sea (Antarctica). Geogr. Fis. Din. Quaternaria 20, 193–198.

Asper, V.L., Smith, W.O., 1999. Particle fluxes during austral spring and summer in the southern Ross Sea, Antarctica. J. Geophys. Res. 104, 5345–5359.

Barbieri, R., D'Onofrio, S., Melis, R., Westall, F., 1999. r-Selected Benthic Foraminifera with Associated Bacterial Colonies in Upper Pleistocene Sediments of the Ross Sea (Antarctica): Implications for Calcium Carbonate Preservation. https://doi.org/10.1016/S0031-0182(98)00191-6.

Bárcena, M.Á., Gersonde, R., Ledesma, S., Fabrés, J., Calafat, A.M., Canals, M., Sierro, F.J., Flores, J.A., 1998. Record of Holocene glacial oscillations in Bransfield Basin as revealed by siliceous microfossil assemblages. Antarct. Sci. 10, 269–285.

Bárcena, M.Á., Isla, E., Plaza, A., Flores, J.A., Sierro, F.J., Masqué, P., Sanchez-Cabeza, J.A., Palanques, A., 2002. Bioaccumulation record and paleoclimatic significance in the Western Bransfield Strait. The last 2000 years. Deep-Sea Res. Pt II 49, 935–950.

Bazin, L., Landais, A., Lemieux-Dudon, B., Toyé Mahamadou Kele, H., Veres, D., Parrenin, F., Martinerie, P., Ritz, C., Capron, E., Lipenkov, V., Loutre, M.-F., Raynaud, D., Vinther, B., Svensson, A., Rasmussen, S.O., Severi, M., Blunier, T., Leuenberger, M., Fischer, H., Masson-Delmotte, V., Chappellaz, J., Wolff, E., 2013. An optimized multi-proxy, multi-site Antarctic ice and gas orbital chronology (AICC2012): 120-800 ka. Clim. Past 9, 1715–1731.

Bentley, M., Hodgson, D.A., Sugden, D., Roberts, S.J., Smith, J.A., Leng, M.J., Bryant, C., 2005. Early Holocene retreat of the George VI ice shelf, antarctic peninsula. Geology 33, 173–176. https://doi.org/10.1130/G21203.1.

Berg, W.J., Van, De, Broeke, M., Van, Den, Ettema, J., Meijgaard, E. Van, 2011. Significant contribution of insolation to Eemian melting of the Greenland ice sheet. Nat. Geosci. 4, 679–683. https://doi.org/10.1038/ngeo1245.

Bergamasco, A., Defendi, V., Budillon, G., Spezie, G., 2004. Downslope flow observations near Cape Adare shelf-break. Antarct. Sci. 16, 199–204. https://doi.org/10.1017/S0954102004001981.

Bergami, C., Capotondi, L., Langone, L., Giglio, F., Ravaioli, M., 2009. Marine micropaleontology distribution of living planktonic foraminifera in the Ross Sea and the Paci fi c sector of the Southern Ocean (Antarctica). Mar. Micropaleontol. 73, 37–48. https://doi.org/10.1016/j.marmicro.2009.06.007.

Bernárdez, P., González-Álvarez, R., Francés, G., Prego, R., Bárcena, M.A., Romero, O.E., 2008. Late Holocene history of the rainfall in the NW Iberian peninsula — evidence from a marine record. J. Mar. Syst. 72, 366–382. https://doi.org/10.1016/j.jmarsys.2007.03.009.

Bertram, R.A., Wilson, D.J., Flierdt, T. van de, Mckay, R.M., Patterson, M.O., Jimenez-Espejo, F.J., Escutia, C., Duke, G.C., Taylor-Silva, B.I., Riesselman, C.R., 2018. Pliocene deglacial event timelines and the biogeochemical response offshore Wilkes Subglacial Basin , East Antarctica. Earth Planet Sci. Lett. 494, 109–116. https://doi.org/10.1016/j.epsl.2018.04.054.

Bianchi, C., Gersonde, R., 2002. The Southern Ocean surface between marine isotope stages 6 and 5d: shape and timing of climate changes. Palaeogeogr. Palaeocl. 187, 151–177.

Bijl, P.K., Sluijs, A., Brinkhuis, H., 2013. A magneto- and chemostratigraphically calibrated dinoflagellate cyst zonation of the early Palaeogene South Pacific Ocean. Earth Sci. Rev. 124, 1–31. https://doi.org/10.1016/j.earscirev.2013.04.010.

Bintanja, R., Oldenborgh, G.J.V.A.N., Katsman, C.A., 2015. The effect of increased fresh water from Antarctic ice shelves on future trends in. Antarctic sea ice 56, 120–126. https://doi.org/10.3189/2015AoG69A001.

Bintanja, R., Oldenborgh, G.J. Van, Drijfhout, S.S., Wouters, B., Katsman, C.A., 2013. Important role for ocean warming and increased ice-shelf melt in Antarctic sea-ice expansion. Nat. Geosci. 6, 376–379. https://doi.org/10.1038/ngeo1767.

Blaga, C.I., Reichart, G.-J., Heiri, O., Sinninghe Damsté, J.S., 2009. Tetraether membrane lipid distributions in water-column particulate matter and sediments: a study of 47 European lakes along a north–south transect. J. Paleolimnol. 41, 523–540. https://doi.org/10.1007/s10933-008-9242-2.

Bonaccorsi, R., Quaia, T., Burckle, L.H., Anderson, R.F., Melis, R., Brambati, A., the 10th ISAES Editorial Team, 2007. C-14 age control of pre- and post-LGM events using N. pachyderma preserved in deep-sea sediments (Ross Sea , Antarctica). In: Cooper, A.K., Raymond, C.R. (Eds.), Antarctica: A Keystone in a Changing World - Online Proceedings for the 10th International Symposium on Antarctic Earth Sciences. USGS Open-File, p. 4. Report 2007-1047, p. Extended Abstract 098.

Bonn, W.J., Gingele, F.X., Grobe, H., Mackensen, A., Ffitterer, D.K., 1998. Paleoproductivity at the Antarctic continental margin: opal and barium records for the last 400 ka. Palaeogeogr. Palaeocl. 139, 195–211.

Bonnet, S., de Vernal, A., Hillaire-Marcel, C., Radi, T., Husum, K., 2010. Variability of sea-surface temperature and sea-ice cover in the Fram Strait over the last two millennia. Mar. Micropaleontol. 74, 59–74. https://doi.org/10.1016/j.marmicro.2009.12.001.

Bracegirdle, T.J., Connolley, W.M., Turner, J., 2008. Antarctic climate change over the twenty first century. J. Geophys. Res. 113, 1–13. https://doi.org/10.1029/2007JD008933.

Bromwich, D.H., Kurtz, D., 1984. Katabatic wind forcing of the Terra Nova Bay polynya. J. Geophys. Res. 89, 3561–3572.

Budillon, G., Tucci, S., Artegiani, A., Spezie, G., 1999. Water masses and suspended matter characteristics of the western Ross Sea. In: Faranda, F.M., Guglielmo, L., Ianora, A. (Eds.), Ross Sea Ecology. Springer-Verlag, Milan, pp. 63–93.

Budillon, G., Gremes Cordero, S., Salusti, E., 2002. On the dense water spreading off the Ross Sea shelf (Southern Ocean). J. Mar. Syst. 35, 207–227. https://doi.org/10.1016/S0924-7963(02)00082-9.

Budillon, G., Pacciaroni, M., Cozzi, S., Rivaro, P., Catalano, G., Ianni, C., Cantoni, C., 2003. An optimum multiparameter mixing analysis of the shelf waters in the Ross Sea. Antarct. Sci. 15, 105–118. https://doi.org/10.1017/S095410200300110X.

Burckle, L.H., Cooke, D.W., 1983. Late Pleistocene Eucampia Antarctica abundance stratigraphy in the Atlantic sector of the Southern Ocean. Micropaleontology 29, 6–10.

Burckle, L.H., Burak, R.W., 1988. Fluctuations in late quaternary diatom abundances: stratigraphy and paleoclimatic implications from subantarctic deep sea cores. Palaeogeogr. Palaeocl. 67, 147–156.

Calvert, S.E., Pedersen, T.F., 2007. Elemental proxies for Palaeoclimatic and palaeoceanographic variability in marine Sediments : interpretation and application. In: Developments in Marine Geology. Elsevier B.V., pp. 567–644. https://doi.org/10.1016/S1572-5480(07)01019-6

Campagne, P., Crosta, X., Schmidt, S., Houssais, M.N., Ther, O., Massé, G., 2016. Sedimentary Response to Sea Ice and Atmospheric Variability over the Instrumental Period off Adélie Land , East Antarctica. Biogeosciences manuscript. https://doi.org/10.5194/bg-2015-610.

Castagno, P., Capozzi, V., DiTullio, G.R., Falco, P., Fusco, G., Rintoul, S.R., Spezie, G., Budillon, G., 2019. Rebound of shelf water salinity in the Ross Sea. Nat. Commun. 10, 5441. https://doi.org/10.1038/s41467-019-13083-8.

Ceccaroni, L., Frank, M., Frignani, M., Langone, L., Ravaioli, M., Mangini, a., 1998. Late

Quaternary fluctuations of biogenic component fluxes on the continental slope of the Ross Sea, Antarctica. J. Mar. Syst. 17, 515–525. https://doi.org/10.1016/S0924-7963(98)00061-X.
Chadwick, M., Allen, C.S., Sime, L.C., Hillenbrand, C.-D., 2020. Analysing the timing of peak warming and minimum winter sea-ice extent in the Southern Ocean during MIS 5e. Quat. Sci. Rev. 229, 106134.
Cheng, H., Edwards, R.L., Broecker, W.S., Denton, G.H., Kong, X., Wang, Y., Zhang, R., Wang, X., 2009. Ice age terminations. Science 326, 248–252. https://doi.org/10.1126/science.1177840.
Church, M.J., DeLong, E.F., Ducklow, H.W., Karner, M.B., Preston, C.M., Karl, D.M., 2003. Abundance and distribution of planktonic archaea and bacteria in the waters west of the antarctic peninsula. Limnol. Oceanogr. 48 https://doi.org/10.4319/lo.2003.48.5.1893, 1893–1902.
Cofaigh, C.Ó., 2012. Ice sheets viewed from the ocean: the contribution of marine science to understanding modern and past ice sheets. Phil. Trans. R. Soc. A 370, 5512–5539. https://doi.org/10.1098/rsta.2012.0398.
Cofaigh, C.Ó., Dowdeswell, J.A., Pudsey, C.J., 2001. Late quaternary iceberg rafting along the antarctic peninsula continental rise and in the Weddell and Scotia seas. Quat. Res. 56, 308–321. https://doi.org/10.1006/qres.2001.2267.
Collins, L.G., Hounslow, M.W., Allen, C.S., Hodgson, D.A., Pike, J., Karloukovski, V.V., 2012. Quaternary geochronology Palaeomagnetic and biostratigraphic dating of marine sediments from the Scotia sea , Antarctica : first identification of the laschamp excursion in the Southern Ocean. Quat. Geochronol. 7, 67–75. https://doi.org/10.1016/j.quageo.2011.10.002.
Comiso, J.C., Nishio, F., 2008. Trends in the sea ice cover using enhanced and compatible AMSR-E , SSM/I. and SMMR data 113, 1–22. https://doi.org/10.1029/2007JC004257.
Crosta, X., Debret, M., Denis, D., Courty, M. a, Ther, O., 2007. Holocene long- and short-term climate changes off Adelie Land, East Antarctica. Geochem. Geophys. Geosy. 8 https://doi.org/10.1029/2007GC001718 n/a-n/a.
Crosta, X., Denis, D., Ther, O., 2008. sea ice seasonality during the Holocene, Adélie land, East Antarctica. Mar. Micropaleontol. 66, 222–232. https://doi.org/10.1016/j.marmicro.2007.10.001.
Crosta, X., Pichon, J.J., Labracherie, M., 1997. Distribution of Chaetoceros resting spores in modern peri-Antarctic sediments. Mar. Micropaleontol. 29, 283–299. https://doi.org/10.1016/S0377-8398(96)00033-3.
Crosta, X., Romero, O., Armand, L.K., Pichon, J., 2005a. The biogeography of major diatom taxa in Southern Ocean sediments : 2. Open ocean related species 223, 66–92. https://doi.org/10.1016/j.palaeo.2005.03.028.
Crosta, X., Shemesh, A., Etourneau, J., Yam, R., Billy, I., Pichon, J.J., 2005b. Nutrient cycling in the Indian sector of the Southern Ocean over the last 50,000 years. Global Biogeochem. Cycles 19, 1–10. https://doi.org/10.1029/2004GB002344.
Crosta, X., Sturm, A., Armand, L., Pichon, J., 2004. Late Quaternary sea ice history in the Indian sector of the Southern Ocean as recorded by diatom assemblages. Mar. Micropaleontol. 50, 209–223. https://doi.org/10.1016/S0377-8398(03)00072-0.
Davey, F.J., Jacobs, S.S., the 10th ISAES Editorial Team, 2007. Influence of submarine morphology on bottom water flow across the western Ross Sea continental margin. In: Cooper, A.K., Raymond, C.R. (Eds.), Antarctica: A Keystone in a Changing World - Online Proceedings for the 10th International Symposium on Antarctic Earth Sciences. USGS Open-File Report 2007-1047. Short Research Paper 067, p. 5.
De Jong, J., Schoemann, V., Maricq, N., Mattielli, N., Langhorne, P., Haskell, T., Tison, J.L., 2013. Iron in land-fast sea ice of McMurdo Sound derived from sediment resuspension and wind-blown dust attributes to primary productivity in the Ross Sea, Antarctica. Mar. Chem. 157, 24–40. https://doi.org/10.1016/j.marchem.2013.07.001.
De Jonge, C., Hopmans, E.C., Zell, C.I., Kim, J., Schouten, S., Damste, J.S.S., 2014. Occurrence and abundance of 6-methyl branched glycerol dialkyl glycerol tetraethers in soils : implications for palaeoclimate reconstruction. Geochem. Cosmochim. Acta 141, 97–112. https://doi.org/10.1016/j.gca.2014.06.013.
De Vernal, A., Henry, M., Matthiessen, J., Mudie, P.J., Rochon, A., Boessenkool, K.P., Eynaud, F., Grøsfjeld, K., Joel, G., Hamel, D., Harland, R., Head, M.J., Kunz-Pirrung, M., Levac, E., Loucheur, V., Peyron, O., Pospelova, V., Radi, T., Turon, J., Voronina, E., 2001. Dinoflagellate cyst assemblages as tracers of sea-surface conditions in the northern North Atlantic , Arctic and sub-Arctic seas : the new "n = 677" data base and its application for quantitative palaeoceanographic reconstruction. J. Quat. Sci. 16, 681–698. https://doi.org/10.1002/jqs.659.
de Vernal, A., Hillaire-Marcel, C., 2000. Sea-ice cover, sea-surface salinity and halo-/thermocline structure of the northwest North Atlantic: modern versus full glacial conditions. Quat. Sci. Rev. 19, 65–85. https://doi.org/10.1016/S0277-3791(99)00055-4.
De Vernal, A., Rochon, A., Fréchette, B., Henry, M., Radi, T., Solignac, S., 2013. Reconstructing past sea ice cover of the Northern Hemisphere from dinocyst assemblages: status of the approach. Quat. Sci. Rev. 79, 122–134. https://doi.org/10.1016/j.quascirev.2013.06.022.
Dearing Crampton-Flood, E., Peterse, F., Sinninghe Damsté, J.S., 2019. Production of branched tetraethers in the marine realm: Svalbard fjord sediments revisited. Org. Geochem. 138, 103907.
DeMaster, D.J., 1981. The supply and accumulation of silica in the marine environment. Geochem. Cosmochim. Acta 45, 1715–1732.
Denis, D., Crosta, X., Barbara, L., Massé, G., Renssen, H., Ther, O., Giraudeau, J., 2010. Sea ice and wind variability during the Holocene in East Antarctica : insight on middle-high latitude coupling. Quat. Sci. Rev. 29, 3709–3719. https://doi.org/10.1016/j.quascirev.2010.08.007.
Denis, D., Crosta, X., Schmidt, S., Carson, D.S., Ganeshram, R.S., Renssen, H., Crespin, J., Ther, O., Billy, I., Giraudeau, J., 2009. Holocene productivity changes off Adélie land (East Antarctica). Paleoceanography 24, PA3207. https://doi.org/10.1029/2008PA001689.
Denis, D., Crosta, X., Zaragosi, S., Romero, O., Martin, B., Mas, V., 2006. Seasonal and subseasonal climate changes recorded in laminated diatom ooze sediments, Adélie Land, East Antarctica. Holocene 16, 1137–1147.
Denton, G.H., Hughes, T.J., 2002. Reconstructing the antarctic ice sheet at the last glacial maximum. Quat. Sci. Rev. 21, 193–202. https://doi.org/10.1016/S0277-3791(01)00090-7.
Deppeler, S.L., Davidson, A.T., 2017. Southern Ocean phytoplankton in a changing climate. Front. Mar. Sci. 4, 40. https://doi.org/10.3389/fmars.2017.00040.
Duprat, L.P.A.M., Bigg, G.R., Wilton, D.J., 2016. Enhanced Southern Ocean marine productivity due to fertilization by giant icebergs. Nat. Geosci. 9, 219–221. https://doi.org/10.1038/ngeo2633.
Dymond, J., Suess, E., Lyle, M., 1992. Barium in deep-sea sediment: a geochemical proxy for paleoproductivity. Paleoceanography 7, 163–181.
Dypvik, H., Harris, N.B., 2001. Geochemical facies analysis of fine-grained siliciclastics using Th/U , Zr/Rb and (Zr+Rb)/Sr ratios. Chem. Geol. 181, 131–146.
Ellegaard, M., Figueroa, R.L., Versteegh, G.J.M., 2013. Dinoflagellate life cycles, strategy and diversity: key foci for future research. In: Lewis, J.M., Marret, F., Bradley, L.R. (Eds.), Biological and Geological Perspectives of Dinoflagellates. The Micropalaeontological Society, Special Publications, London, pp. 249–261.
Elling, F.J., Könneke, M., Lipp, J.S., Becker, K.W., Gagen, E.J., Hinrichs, K.-U., 2014. Effects of growth phase on the membrane lipid composition of the thaumarchaeon *Nitrosopumilus maritimus* and their implications for archaeal lipid distributions in the marine environment. Geochem. Cosmochim. Acta 141, 579–597. https://doi.org/10.1016/j.gca.2014.07.005.
Esper, O., Gersonde, R., 2014. New tools for the reconstruction of Pleistocene Antarctic sea ice. Palaeogeogr. Palaeocl. 399, 260–283. https://doi.org/10.1016/j.palaeo.2014.01.019.
Esper, O., Gersonde, R., Kadagies, N., 2010. Diatom distribution in southeastern Pacific surface sediments and their relationship to modern environmental variables. Palaeogeogr. Palaeocl. 287, 1–27. https://doi.org/10.1016/j.palaeo.2009.12.006.
Esper, O., Zonneveld, K.A.F., 2007. The potential of organic-walled dinoflagellate cysts for the reconstruction of past sea-surface conditions in the Southern Ocean. Mar. Micropaleontol. 65, 185–212. https://doi.org/10.1016/j.marmicro.2007.07.002.
Esper, O., Zonneveld, K.A.F., 2002. Distribution of organic-walled dinoflagellate cysts in surface sediments of the Southern Ocean (eastern Atlantic sector) between the subtropical front and the Weddell Gyre. Mar. Micropaleontol. 46, 177–208 https://doi.org/https://doi.org/10.1016/S0377-8398(02)00041-5.
Fernandez-Mendez, M., Katlein, C., Rabe, B., Nicolaus, M., Peeken, I., Bakker, K., Flores, H., Boetius, A., 2015. Photosynthetic production in the central Arctic Ocean during the record sea-ice minimum in 2012. Biogeosciences 12, 3525–3549. https://doi.org/10.5194/bg-12-3525-2015.
Ferrari, R., Jansen, M.F., Adkins, J.F., Burke, A., Stewart, A.L., Thompson, A.F., 2014. Antarctic sea ice control on ocean circulation in present and glacial climates. P. Natl. Acad. Sci. USA 111, 8753–8758. https://doi.org/10.1073/pnas.1323922111.
Ferry, A.J., Crosta, X., Quilty, P.G., Fink, D., Howard, W., Armand, L.K., 2015. First records of winter sea-ice concentration in the southwest Pacific sector of the Southern Ocean. MS. Paleoceanography. https://doi.org/10.1002/2014PA002764 n/a-n/a.
Fitch, D.T., Moore, J.K., 2007. Wind speed influence on phytoplankton bloom dynamics in the Southern Ocean marginal ice zone. J. Geophys. Res. 112, C08006. https://doi.org/10.1029/2006JC004061.
François, R., Altabet, M.A., Yu, E.-F., Sigman, D.M., Bacon, M.P., Frank, M., Bohrmann, G., Bareille, G., Labeyrie, L.D., 1997. Contribution of Southern Ocean surface-water stratification to low atmospheric CO2 concentrations during the last glacial period. Nature 389, 929–935. https://doi.org/10.1038/40073.
Fryxell, G.A., Prasad, A.K.S.K., 1990. *Eucampia antarctica* var. *recta* (Mangin) stat. nov. (Biddulphiaceae, Bacillariopyceae): life stages at the Weddel Sea ice edge. Phycologia 29 (1), 27–38.
Garibotti, I.A., Vernet, M., Smith, R.C., Ferrario, M.E., 2005. Interannual variability in the distribution of the phytoplankton standing stock across the seasonal sea-ice zone west of the Antarctic Peninsula. J. Plankton Res. 27, 825–843. https://doi.org/10.1093/plankt/fbi056.
Garrison, D.L., Close, A.R., 1993. Winter Ecology of the Sea Ice Biota in Weddell Sea Pack Ice.
Garrison, D.L., Gibson, A., Coale, S.L., Gowing, M.M., Okolodkov, Y.B., Fritsen, C.H., Jeffries, M.O., 2005. Sea-ice microbial communities in the Ross Sea: autumn and summer biota. Mar. Ecol. Prog. Ser. 300, 39–52. https://doi.org/10.3354/meps300039.
Gersonde, R., Abelman, A., Brathauer, U., Becquey, S., Bianchi, C., Cortese, G., Grobe, H., Kuhn, G., Niebler, H.-S., Segl, M., Sieger, R., Zielinski, U., Fütterer, D.K., 2003. Last glacial sea surface temperatures and sea-ice extent in the Southern Ocean (Atlantic-Indian sector): a multiproxy approach. Paleoceanography 18, 1–18. https://doi.org/10.1029/2002PA000809.
Gersonde, R., Crosta, X., Abelmann, A., Armand, L., 2005. Sea-surface temperature and sea ice distribution of the Southern Ocean at the EPILOG Last Glacial Maximum—a circum-Antarctic view based on siliceous microfossil records. Quat. Sci. Rev. 24, 869–896. https://doi.org/10.1016/j.quascirev.2004.07.015.

Gersonde, R., Zielinski, U., 2000. The reconstruction of late Quaternary Antarctic sea-ice distribution — the use of diatoms as a proxy for sea-ice. Palaeogeogr. Palaeocl. 162, 263–286.
Gordon, A.L., Orsi, A.H., Muench, R., Huber, B.A., Zambianchi, E., Visbeck, M., 2009. Western Ross Sea continental slope gravity currents. Deep-Sea Res. Pt II 56, 796–817. https://doi.org/10.1016/j.dsr2.2008.10.037.
Grigorov, I., Rigual-Hernandez, A.S., Honjo, S., Kemp, A.E.S., Armand, L.K., 2014. Settling fluxes of diatoms to the interior of the Antarctic circumpolar current along 170 °W. Deep-Sea Res. Pt I 93, 1–13. https://doi.org/10.1016/j.dsr.2014.07.008.
Grobe, H., Mackensen, A., 1992. Late quaternary climatic cycles as recorded in sediments from the antarctic continental margin. In: Kennett, J.P., Warkne, D.A. (Eds.), The Antarctic Paleoenvironment: A Perspective on Global Change - Part One. American Geophysical Union, Antarctic Research Series, Washington, D.C., pp. 349–376
Hannah, M.J., 2006. The palynology of ODP site 1165, Prydz Bay, East Antarctica : a record of Miocene glacial advance and retreat. Palaeogeogr. Palaeocl. 231, 120–133. https://doi.org/10.1016/j.palaeo.2005.07.029.
Hannah, M.J., Fielding, C.R., 2001. Chronostratigraphy of the CRP-3 Drillhole , Victoria Land Basin. Antarctica © Terra Antartica Publication.
Harloff, J., Mackensen, A., 1997. Recent benthic foraminiferal associations and ecology of the Scotia Sea and Argentine Basin. Mar. Micropaleontol. 31, 1–29.
Hartman, J.D., Bijl, P.K., Sangiorgi, F., 2018a. A review of the ecological affinities of marine organic microfossils from a Holocene record offshore of Adélie Land (East Antarctica). J. Micropalaeontol. 37, 445–497.
Hartman, J.D., Sangiorgi, F., Bijl, P.K., Versteegh, G.J.M., 2018b. Nucicla umbiliphora gen. et sp. nov.: a Quaternary peridinioid dinoflagellate cyst from the Antarctic margin. Palynology 1–10. https://doi.org/10.1080/01916122.2018.1430070.
Haumann, F.A., Gruber, N., Münnich, M., Frenger, I., Kern, S., 2016. Sea-ice transport driving Southern Ocean salinity and its recent trends. Nature 537, 89–92. https://doi.org/10.1038/nature19101.
Heinrich, H., 1988. Origin and consequences of cyclic ice rafting in the Northeast Atlantic ocean during the past 130,000 years. Quat. Res. 29, 142–152.
Higgins, M.B., Robinson, R.S., Carter, S.J., Pearson, A., 2010. Evidence from chlorin nitrogen isotopes for alternating nutrient regimes in the Eastern Mediterranean Sea. Earth Planet Sci. Lett. 290, 102–107. https://doi.org/10.1016/j.epsl.2009.12.009.
Higgins, M.B., Robinson, R.S., Husson, J.M., Carter, S.J., Pearson, A., 2012. Dominant eukaryotic export production during ocean anoxic events reflects the importance of recycled NH_4^+. Proc. Natl. Acad. Sci. Unit. States Am. 109 (7), 2269–2274. https://doi.org/10.1073/pnas.1104313109.
Hillenbrand, C.-D., Fütterer, D.K., 2001. 23 . Neogene to Quaternary deposition of opal on the continental rise west of the Antarctic Peninsula, ODP Leg 178 , Sites 1095 , 1096 , and 1101. In: Barker, P.F., Camerlenghi, A., Acton, G.D., Ramsay, A.T.S. (Eds.), Proceedings of the Ocean Drilling Program, Scientific Results, pp. 1–33.
Hillenbrand, C.-D., Grobe, H., Diekmann, B., Kuhn, G., Fütterer, D.K., 2003. Distribution of clay minerals and proxies for productivity in surface sediments of the Bellingshausen and Amundsen seas (West Antarctica) - relation to modern environmental conditions. Mar. Geol. 193, 253–271.
Hillenbrand, C.-D., Kuhn, G., Frederichs, T., 2009. Record of a Mid-Pleistocene depositional anomaly in West Antarctic continental margin sediments : an indicator for ice-sheet collapse? Quat. Sci. Rev. 28, 1147–1159.
Hopmans, E.C., Schouten, S., Sinninghe Damsté, J.S., 2016. Organic Geochemistry the effect of improved chromatography on GDGT-based palaeoproxies. Org. Geochem. 93, 1–6. https://doi.org/10.1016/j.orggeochem.2015.12.006.
Hopmans, E.C., Weijers, J.W.H., Schefuß, E., Herfort, L., Sinninghe Damsté, J.S., Schouten, S., 2004. A novel proxy for terrestrial organic matter in sediments based on branched and isoprenoid tetraether lipids. Earth Planet Sci. Lett. 224, 107–116. https://doi.org/10.1016/j.epsl.2004.05.012.
Howe, J.A., Harland, R., Pudsey, C.J., 2002. Dinoflagellate cyst evidence for quaternary palaeoceanographic change in the northern Scotia sea, south Atlantic ocean. Mar. Geol. 191, 55–69. https://doi.org/10.1016/S0025-3227(02)00498-X.
Huguet, C., de Lange, G.J., Gustafsson, Ö., Middelburg, J.J., Sinninghe Damsté, J.S., Schouten, S., 2008. Selective preservation of soil organic matter in oxidized marine sediments (Madeira Abyssal Plain). Geochem. Cosmochim. Acta 72, 6061–6068. https://doi.org/10.1016/j.gca.2008.09.021.
Huguet, C., Kim, J., Lange, G.J. De, Sinninghe, J.S., Schouten, S., 2009. Organic Geochemistry Effects of long term oxic degradation on the U K 37 , TEX 86 and BIT organic proxies. Org. Geochem. 40, 1188–1194. https://doi.org/10.1016/j.orggeochem.2009.09.003.
Hurley, S.J., Elling, F.J., Könneke, M., Buchwald, C., Wankel, S.D., Santoro, A.E., Lipp, J.S., Hinrichs, K.-U., Pearson, A., 2016. Influence of ammonia oxidation rate on thaumarchaeal lipid composition and the TEX86 proxy. P. Natl. Acad. Sci. USA 113, 7762–7767. https://doi.org/10.1073/pnas.1518534113.
Jacobs, S.S., 1991. On the nature and significance of the Antarctic Slope. Front. Mar. Chem. 35, 9–24. https://doi.org/10.1016/S0304-4203(09)90005-6.
Jacobs, S.S., 1989. Marine controls on modern sedimentation on the Antarctic continental shelf. Mar. Geol. 85, 121–153.
Jacobs, S.S., Amos, A.F., Bruchhausen, P.M., 1970. Ross sea oceanography and antarctic bottom water formation. Deep-Sea Res. 17, 935–962. https://doi.org/10.1016/0011-7471(70)90046-X.
Jacobs, S.A., Fairbanks, R.C., Horibe, Y., 1985. Origin and evolution of water masses near the Antarctc continental margin: evidence from $H_2^{18}O/H_2^{16}O$ ratios in seawater. In: Jacobs, S.S. (Ed.), Oceanology of the Antarctic Continental Shelf, vol. 3, pp. 59–85.
Jimenez-Espejo, F.J., Presti, M., Kuhn, G., Mckay, R., Crosta, X., Escutia, C., Lucchi, R.G., Yoshimura, T., Ortega, M., Macrì, P., Caburlotto, A., Santis, L. De, 2020. Late Pleistocene oceanographic and depositional variations along the Wilkes Land margin (East Antarctica) reconstructed with geochemical proxies in deep-sea sediments. Global Planet. Change 184, 103045. https://doi.org/10.1016/j.gloplacha.2019.103045.
Johansen, J.R., Fryxell, G.A., 1985. The genus *Thalassiosira* (Bacillariophyceae): studies on species occurring south of the Antarctic Convergence Zone. Phycologia 24 (2), 155–179.
Jones, B., Manning, D.A.C., 1994. Comparison of geochemical indices used for the interpretation of palaeoredox conditions in ancient mudstones. Chem. Geol. 111, 111–129. https://doi.org/10.1016/0009-2541(94)90085-X.
Jorissen, F.J., de Stigter, H.C., Widmark, J.G.V., 1995. A conceptual model explaining benthic foraminiferal microhabitats. Mar. Micropaleontol. 26, 3–15. https://doi.org/10.1016/0377-8398(95)00047-X.
Jorissen, F.J., Fontanier, C., Thomas, E., 2007. Paleoceanographical proxies based on deep-sea benthic foraminiferal assemblage characteristics. In: Developments in Marine Geology. Elsevier B.V., pp. 263–325. https://doi.org/10.1016/S1572-5480(07)01012-3
Kaczmarska, I., Barbrick, N.E., Ehrman, J.M., Cant, G.P., 1993. Eucampia index as an indicator of the late Pleistocene oscillations of the winter sea-ice extent at the ODP leg 119 site 745B at the kerguelen plateau. Hydrobiologia 269/270, 103–112.
Kalanetra, K.M., Bano, N., Hollibaugh, J.T., 2009. Ammonia-oxidizing archaea in the Arctic ocean and antarctic coastal waters. Environ. Microbiol. 11, 2434–2445. https://doi.org/10.1111/j.1462-2920.2009.01974.x.
Kay, J.E., Holland, M.M., Jahn, A., 2011. Inter - Annual to Multi - Decadal Arctic Sea Ice Extent Trends in a Warming World 38, pp. 2–7. https://doi.org/10.1029/2011GL048008.
Kim, J.-H., Crosta, X., Willmott, V., Renssen, H., Bonnin, J., Helmke, P., Schouten, S., Sinninghe Damsté, J.S., 2012. Holocene subsurface temperature variability in the eastern Antarctic continental margin. Geophys. Res. Lett. 39, L06705. https://doi.org/10.1029/2012GL051157.
Klump, J., Hebbeln, D., Wefer, G., 2000. The impact of sediment provenance on barium-based productivity estimates. Mar. Geol. 169, 259–271.
Koga, Y., Morii, H., Akagawa-Matsushita, M., Ohga, M., 1998. Correlation of polar lipid composition with 16S rRNA Phylogeny in methanogens. Further analysis of lipid component parts. Biosci. Biotechnol. Biochem. 62, 230–236. https://doi.org/10.1271/bbb.62.230.
Kunz-Pirrung, M., Matthiessen, J., De Vernal, A., 2001. Relationships between dinoflagellate cyst assemblages in surface sediment and hydrographic conditions in the Bering and Chukchi seas. J. Quat. Sci. 16, 667–680. https://doi.org/10.1002/jqs.652.
Leventer, A., 1998. The fate of Antarctic “sea ice diatoms” and their use as paleoenvironmental indicators. Antarct. Res. 73, 121–137.
Leventer, A., Domack, E.W., Ishman, S.E., Brachfeld, S., McClennen, C.E., Manley, P., 1996. Productivity cycles of 200-300 years in the Antarctic Peninsula region: understanding linkages among the sun, atmosphere, oceans, sea-ice and biota. Geol. Soc. Am. Bull. 108, 1626–1644. https://doi.org/10.1130/0016-7606(1996)108<1626.
Lindenberg, H.G., Auras, A., 1984. Distribution of arenaceous foraminifera in depth profiles of the Southern Ocean (Kerguelen Plateau area). Palaeogeogr. Palaeocl. 48, 61–106.
Liu, Y., Moore, J.C., Cheng, X., Gladstone, R.M., Bassis, J.N., Liu, H., Wen, J., Hui, F., 2015. Ocean-driven thinning enhances iceberg calving and retreat of Antarctic ice shelves. P. Natl. Acad. Sci. USA 112, 3263–3268. https://doi.org/10.1073/pnas.1415137112.
Lizotte, M.P., 2001. The contributions of sea ice Algae to antarctic marine primary production. Am. Zool. 41, 57–73 https://doi.org/10.1668/0003-1569(2001)041[0057:TCOSIA]2.0.CO;2.
Locarnini, R.A., Mishonov, A.V., Antonov, J.I., Boyer, T.P., Garcia, H.E., Baranova, O.K., Zweng, M.M., Johnson, D.R., 2010. World ocean Atlas 2009. In: Temperature. NOAA Atlas NESDIS 68, vol. 1. U.S. Government Printing Office, Washington, D.C.
Lucchi, R.G., Rebesco, M., Camerlenghi, A., Busetti, M., Tomadin, L., Villa, G., Persico, D., Morigi, C., Bonci, M.C., Giorgetti, G., 2002. Mid-late Pleistocene glacimarine sedimentary processes of a high-latitude, deep-sea sediment drift (Antarctic Peninsula Pacific margin). Mar. Geol. 189, 343–370.
Lüthi, D., Le Floch, M., Bereiter, B., Blunier, T., Barnola, J.-M., Siegenthaler, U., Raynaud, D., Jouzel, J., Fischer, H., Kawamura, K., Stocker, T.F., 2008. High-resolution carbon dioxide concentration record 650,000-800,000 years before present. Nature 453, 379–382. https://doi.org/10.1038/nature06949.
Mackensen, A., Grobe, H., Kuhn, G., Fiitterer, D.K., 1990. Benthic foraminiferal assemblages from the eastern Weddell Sea between 68 and 73 ° S : distribution , ecology and fossilization potential. Mar. Micropaleontol. 16, 241–283.
Malinverno, E., Maffioli, P., Gariboldi, K., 2016. Latitudinal distribution of extant fossilizable phytoplankton in the Southern Ocean : planktonic provinces , hydrographic fronts and palaeoecological perspectives. Mar. Micropaleontol. 123, 41–58. https://doi.org/10.1016/j.marmicro.2016.01.001.
Marret, F., Bradley, L., Vernal, A. de, Hardy, W., Kim, S.-Y., Mudie, P., Penaud, A., Pospelova, V., Price, A.M., Radi, T., Rochon, A., 2019. From bi-polar to regional distribution of modern dinoflagellate cysts, an overview of their biogeography. Mar. Micropaleontol. https://doi.org/10.1016/j.marmicro.2019.101753 (in press).
Marret, F., De Vernal, A., 1997. Dinoflagellate cyst distribution in surface sediments of the southern Indian Ocean. Mar. Micropaleontol. 29, 367–392. https://

doi.org/10.1016/S0377-8398(96)00049-7.
Marret, F., De Vernal, A., Benderra, F., Harland, R., 2001. Late quaternary sea-surface conditions at DSDP Hole 594 in the Southwest Pacific Ocean based on dinoflagellate cyst assemblages. J. Quat. Sci. 16, 739–751. https://doi.org/10.1002/jqs.648.
Martínez-Garcia, A., Rosell-Melé, A., Geibert, W., Gersonde, R., Masqué, P., Gaspari, V., Barbante, C., 2009. Links between iron supply, marine productivity, sea surface temperature, and CO2 over the last 1.1 Ma. Paleoceanography 24, 1–14. https://doi.org/10.1029/2008PA001657.
McGillicuddy, D.J., Sedwick, P.N., Dinniman, M.S., Arrigo, K.R., Bibby, T.S., Greenan, B.J.W., Hofmann, E.E., Klinck, J.M., Smith, W.O., Mack, S.L., Marsay, C.M., Sohst, B.M., Van Dijken, G.L., 2015. Iron supply and demand in an Antarctic shelf ecosystem. Geophys. Res. Lett. 42, 8088–8097. https://doi.org/10.1002/2015GL065727.
McKay, N.P., Overpeck, J.T., Otto-Bliesner, B.L., 2011. The role of ocean thermal expansion in Last Interglacial sea level rise. Geophys. Res. Lett. 38, 4–9. https://doi.org/10.1029/2011GL048280.
McManus, J., Berelson, W.M., Klinkhammer, G.P., Johnson, K.S., Coale, K.H., Anderson, R.F., Kumar, N., Burdige, D.J., Hammond, D.E., Brumsack, H.J., McCorkle, D.C., Rushdi, A., 1998. Geochemistry of barium in marine sediments : implications for its use as a paleoproxy. Geochem. Cosmochim. Acta 62, 3453–3473. https://doi.org/10.1016/S0016-7037(98)00248-8.
Meyers, S.R., Sageman, B.B., 2007. Quantification of deep-time orbital forcing by average spectral misfit. Am. J. Sci. 307, 773–792. https://doi.org/10.2475/05.2007.01.
Meyers, S.R., Sageman, B.B., Arthur, M.A., 2012. Obliquity forcing of organic matter accumulation during Oceanic Anoxic. Event 2 27, 1–19. https://doi.org/10.1029/2012PA002286.
Mezgec, K., Stenni, B., Crosta, X., Masson-Delmotte, V., Baroni, C., Braida, M., Ciardini, V., Coliza, E., Melis, R., Salvatore, M.C., Scarchilli, C., Traversi, R., Udisti, R., Frezzotti, M., 2017. Holocene sea ice variability driven by wind and polynya efficiency in the Ross Sea. Nat. Commun. 8, 1334. https://doi.org/10.1038/s41467-017-01455-x.
Minzoni, R.T., Anderson, J.B., Fernandez, R., Wellner, J.S., 2015. Marine record of Holocene climate, ocean, and cryosphere interactions: Herbert sound, James Ross Island, Antarctica. Quat. Sci. Rev. 129, 239–259. https://doi.org/10.1016/j.quascirev.2015.09.009.
Mollenhauer, G., Basse, A., Kim, J.H., Sinninghe Damsté, J.S., Fischer, G., 2015. A four-year record of UK'37- and TEX86-derived sea surface temperature estimates from sinking particles in the filamentous upwelling region off Cape Blanc, Mauritania. Deep-Sea Res. Pt I 97, 67–79. https://doi.org/10.1016/j.dsr.2014.11.015.
Mortlock, R.A., Charles, C.D., Froelich, P.N., Zibello, M.A., Saltzman, J., Hays, J.D., Burckle, L.H., 1991. Evidence for lower productivity in the Antarctic Ocean during the last glaciation. Nature 351, 220–223.
Mudie, P.J., 1992. Circum-Arctic Quaternary and Neogene marine palynofloras: paleoecology and statistical analysis. In: Head, M.J., Wrenn, J.H. (Eds.), *Neogene and Quaternary Dinoflagellate Cysts and Acritarchs:* Salt Lake City, UT. Publishers Press, pp. 347–390.
Mudie, P.J., Harland, R., 1996. Chapter 21. Aquatic quaternary. In: Jansonius, J., McGregor, D.C. (Eds.), Palynology: Principles and Applications, vol. 2. American Association of Stratigraphic Palynologists Foundation, Dallas, Texas, pp. 843–877.
Mudie, P.J., Leroy, S.A.G., Marret, F., Gerasimenko, N.P., Kholeif, S.E.A., Sapelko, T., Filipova-Marinova, M., 2011. Nonpollen palynomorphs: indicators of salinity and environmental change in the Caspian – black Sea – Mediterranean corridor. In: Buynevich, I.V., Yanko-Hombach, V., Gilbert, A.S., Martin, R.E. (Eds.), Geology and Geoarchaeology of the Black Sea Region: beyond the Flood Hypothesis. The Geological Society of America Special Paper, pp. 89–115. https://doi.org/10.1130/2011.2473(07.
Mudie, P.J., Marret, F., Rochon, a., Aksu, A.E., 2010. Non-pollen palynomorphs in the black sea corridor. Veg. Hist. Archaeobotany 19, 531–544. https://doi.org/10.1007/s00334-010-0268-9.
Murphy, E.J., Thorpe, S.E., Tarling, G.A., Watkins, J.L., Fielding, S., Underwood, P., 2017. Restricted regions of enhanced growth of Antarctic krill in the circumpolar Southern Ocean. Sci. Rep. 7, 6963. https://doi.org/10.1038/s41598-017-07205-9.
Murray, A.E., Preston, C.M., Massana, R., Taylor, T.L., Blakis, A., Wu, K., Delong, E.F., 1998. Seasonal and spatial variability of bacterial and archaeal assemblages in the coastal waters near Anvers Island, Antarctica. Appl. Environ. Microbiol. 64, 2585–2595.
Naafs, B.D.A., Inglis, G.N., Zheng, Y., Amesbury, M.J., Biester, H., Bindler, R., Blewett, J., Burrows, M.A., del Castillo Torres, D., Chambers, F.M., Cohen, A.D., Evershed, R.P., Feakins, S.J., Gałka, M., Gallego-Sala, A., Gandois, L., Gray, D.M., Hatcher, P.G., Honorio Coronado, E.N., Hughes, P.D.M., Huguet, M., Könönen, M., Laggoun-Défarge, F., Lähteenoja, O., Lamentowitz, M., Marchant, R., McClymont, E., Pontevedra-Pombal, X., Ponton, C., Pourmand, A., Rizzuti, A.M., Rochefort, L., Schellekens, J., De Vleeschouwer, F., Pancost, R.D., 2017. Introducing global peat-specific temperature and pH calibrations based on brGDGT bacterial lipids. Geochem. Cosmochim. Acta 208, 285–301.
Nelson, D.M., DeMaster, D.J., Dunbar, B., Smith Jr., W.O., 1996. Cycling of organic carbon and biogenic silica in the Southern Ocean: estimates of water-column and sedimentary fluxes on the Ross Sea continental shelf. J. Geophys. Res. 101, 18519–18532.
Notz, D., Marotzke, J., 2012. Observations Reveal External Driver for Arctic Sea-Ice Retreat 39, pp. 1–6. https://doi.org/10.1029/2012GL051094.
Nylen, T.H., Fountain, A.G., Doran, P.T., 2004. Climatology of katabatic winds in the McMurdo dry valleys, southern Victoria Land, Antarctica. J. Geophys. Res. 109, D03114. https://doi.org/10.1029/2003JD003937.
Orsi, A.H., Whitworth III, T., Nowlin Jr., W.D., 1995. On the meridional extent and fronts of the Antarctic Circumpolar Current. Deep-Sea Res. Pt I 42 (5), 641–673.
Orsi, A.H., Wiederwohl, C.L., 2009. A recount of Ross Sea waters. Deep-Sea Res. Pt II 56, 778–795. https://doi.org/10.1016/j.dsr2.2008.10.033.
Past Interglacials Working Group of PAGES, 2016. Interglacials of the last 800.000 years. Rev. Geophys. 54 https://doi.org/10.1002/2015RG000482.
Paolo, F.S., Fricker, H.A., Padman, L., 2015. Volume loss from Antarctic ice shelves is accelerating. Science 348, 327–332. https://doi.org/10.1126/science.aaa0940.
Park, J.-Y., Kug, J.-S., Bader, J., Rolph, R., Kwon, M., 2015. Amplified Arctic warming by phytoplankton under greenhouse warming. P. Natl. Acad. Sci. USA 112, 5921–5926. https://doi.org/10.1073/pnas.1416884112.
Parkinson, C.L., 2019. A 40-y record reveals gradual Antarctic sea ice increases followed by decreases at rates far exceeding the rates seen in the Arctic. P. Natl. Acad. Sci. USA 116, 14414–14423. https://doi.org/10.1073/pnas.1906556116.
Parkinson, C.L., Cavalieri, D.J., 2012. The Cryosphere Antarctic Sea Ice Variability and Trends. https://doi.org/10.5194/tc-6-871-2012, 1979 – 2010 871–880.
Peck, L.S., Barnes, D.K.A., Cook, A.J., Fleming, A.H., Clarke, A., 2010. Negative feedback in the cold : ice retreat produces new carbon sinks in Antarctica. Global Change Biol. 16, 2614–2623. https://doi.org/10.1111/j.1365-2486.2009.02071.x.
Peloquin, J.A., Smith Jr., W.O., 2007. Phytoplankton blooms in the Ross Sea, Antarctica: Interannual variability in magnitude, temporal patterns, and composition. J. Geophys. Res. 112, C08013. https://doi.org/10.1029/2006JC003816.
Peterse, F., Kim, J., Schouten, S., Klitgaard, D., Koç, N., Sinninghe, J.S., 2009. Constraints on the application of the MBT/CBT palaeothermometer at high latitude environments (Svalbard , Norway). Org. Geochem. 40, 692–699. https://doi.org/10.1016/j.orggeochem.2009.03.004.
Petit, R.J., Raynaud, D., Basile, I., Chappellaz, J., Ritz, C., Delmotte, M., Legrand, M., Lorius, C., Pe, L., 1999. Climate and atmospheric history of the past 420,000 years from the Vostok ice core, Antarctica. Nature 399. https://doi.org/10.1038/20859, 429–413.
Pieńkowski, A.J., Marret, F., Scourse, J.D., Thomas, D.N., 2013. Organic-walled microfossils from the north-west Weddell Sea, Antarctica: records from surface sediments after the collapse of the Larsen-A and Prince Gustav Channel ice shelves. Antarct. Sci. 25, 565–574 https://doi.org/Doi 10.1017/S0954102012001186.
Prebble, J.G., Crouch, E.M., Carter, L., Cortese, G., Bostock, H., Neil, H., 2013. An expanded modern dinoflagellate cyst dataset for the Southwest Pacific and Southern Hemisphere with environmental associations. Mar. Micropaleontol. 101, 33–48. https://doi.org/10.1016/j.marmicro.2013.04.004.
Pudsey, C.J., Camerlenghi, A., 1998. Glacial-interglacial deposition on a sediment drift on the Pacific margin of the Antarctic Peninsula. Antarct. Sci. 10, 286–308.
Pudsey, C.J., Howe, J.A., 1998. Quaternary history of the antarctic circumpolar Current : evidence from the Scotia sea. Mar. Geol. 148, 83–112.
Pugh, R.S., Mccave, I.N., Hillenbrand, C.D., Kuhn, G., 2009. Circum-Antarctic age modelling of Quaternary marine cores under the Antarctic Circumpolar Current : ice-core dust – magnetic correlation. Earth Planet Sci. Lett. 284, 113–123. https://doi.org/10.1016/j.epsl.2009.04.016.
Qin, W., Carlson, L.T., Armbrust, E.V., Devol, A.H., Moffett, J.W., Stahl, D.A., Ingalls, A.E., 2015. Confounding effects of oxygen and temperature on the TEX $_{86}$ signature of marine Thaumarchaeota. P. Natl. Acad. Sci. USA 112, 10979–10984. https://doi.org/10.1073/pnas.1501568112.
Radi, T., de Vernal, A., 2008. Dinocysts as proxy of primary productivity in mid-high latitudes of the Northern Hemisphere. Mar. Micropaleontol. 68, 84–114. https://doi.org/10.1016/j.marmicro.2008.01.012.
Railsback, L.B., Gibbard, P.L., Head, M.J., Voarintsoa, N.R.G., Toucanne, S., 2015. An optimized scheme of lettered marine isotope substages for the last 1.0 million years, and the climatostratigraphic nature of isotope stages and substages. Quat. Sci. Rev. 111, 94–106. https://doi.org/10.1016/j.quascirev.2015.01.012.
Reichart, G., Brinkhuis, H., 2003. Late quaternary Protoperidinium cysts as indicators of paleoproductivity in the northern Arabian sea. Mar. Micropaleontol. 49, 303–315. https://doi.org/10.1016/S0377-8398(03)00050-1.
Rembauville, M., Blain, S., Armand, L., Quéguiner, B., Salter, I., 2015. Export fluxes in a naturally iron-fertilized area of the Southern Ocean – Part 2 : importance of diatom resting spores and faecal pellets for export. Biogeosciences 12, 3171–3195. https://doi.org/10.5194/bg-12-3171-2015.
Rembauville, M., Manno, C., Tarling, G.A., Blain, S., Salter, I., 2016. Strong contribution of diatom resting spores to deep-sea carbon transfer in naturally iron-fertilized waters downstream of South Georgia. Deep-Sea Res. Pt I 115, 22–35. https://doi.org/10.1016/j.dsr.2016.05.002.
Ribeiro, S., Amorim, A., Abrantes, F., Ellegaard, M., 2016. Environmental change in the Western Iberia Upwelling Ecosystem since the preindustrial period revealed by dinoflagellate cyst records. Holocene 26, 874–889. https://doi.org/10.1177/0959683615622548.
Riesselman, C.R., Dunbar, R.B., 2013. Diatom evidence for the onset of Pliocene cooling from AND-1B, McMurdo Sound, Antarctica. Palaeogeogr. Palaeocl. 369, 136–153. https://doi.org/10.1016/j.palaeo.2012.10.014.
Rigual-Hernández, A.S., Colmenero-Hidalgo, E., Martrat, B., Bárcena, M.A., Vernal, A. de, Sierro, F.J., Flores, J.A., Grimalt, J.O., Henry, M., Lucchi, R.G., 2017. Svalbard ice-sheet decay after the Last Glacial Maximum: new insights from micro-palaeontological and organic biomarker paleoceanographical reconstructions.

Palaeogeogr. Palaeocl. 465, 225–236. https://doi.org/10.1016/j.palaeo.2016.10.034.
Rintoul, S.R., 2018. The global influence of localized dynamics in the Southern Ocean. Nature 558, 209–218.
Robinson, R.S., Kienast, M., Albuquerque, A.L., Altabet, M., Contreras, S., De Pol Holz, R., Dubois, N., Francois, R., Galbraith, E., Hsu, T.C., Ivanochko, T., Jaccard, S., Kao, S.J., Krefer, T., Kienast, S., Lehmann, M., Martinez, P., McCarthy, M., Möbius, J., Pedersen, T., Quan, T.M., Ryabenko, E., Schmittner, A., Schneider, R., Schneider-Mor, A., Shigemitsu, M., Sinclair, D., Somes, C., Studer, A., Thunell, R., Yang, J.Y., 2012. A review of nitrogen isotopic alteration in marine sediments. Paleoceanography 27, PA4203. https://doi.org/10.1029/2012PA002321.
Sabbatini, A., Morigi, C., Ravaioli, M., Negri, A., 2004. Abyssal benthic foraminifera IN the polar front region (pacific sector): faunal composition , standing stock and size structure. Chem. Ecol. 20, S117–S129.
Salter, I., Kemp, A.E.S., Moore, C.M., Lampitt, R.S., Wolff, G.A., Holtvoeth, J., 2012. Diatom resting spore ecology drives enhanced carbon export from a naturally iron-fertilized bloom in the. Southern Ocean 26, 1–17. https://doi.org/10.1029/2010GB003977.
Sarmiento, J.L., Slater, R., Barber, R., Bopp, L., Doney, S.C., Hirst, A.C., Kleypas, J., Matear, R., Mikolajewicz, U., Monfray, P., Soldatov, V., Spall, S.A., Stouffer, R., 2004. Response of ocean ecosystems to climate warming. Global Biogeochem. Cycles 18, 1–23. https://doi.org/10.1029/2003GB002134.
Schouten, S., Hopmans, E.C., E S, M., 2002. Distributional variations in marine crenarchaeotal membrane lipids : a new tool for reconstructing ancient sea water temperatures ? Earth Planet Sci. Lett. 204, 265–274. https://doi.org/10.1016/S0012-821X(02)00979-2.
Schouten, S., Hopmans, E.C., Sinninghe Damsté, J.S., 2013. The organic geochemistry of glycerol dialkyl glycerol tetraether lipids: a review. Org. Geochem. 54, 19–61. https://doi.org/10.1016/j.orggeochem.2012.09.006.
Schrader, H.J., Gersonde, R., 1978. Diatoms and silicoflagellates. Micropaleontological counting methods and techniques: an exercise on an eight metres section of the Lower Pliocene of Capo Rosello, Sicily. Utrecht Bull. Micropaleontol. 17, 129–176.
Sedwick, P.N., DiTullio, G.R., Mackey, D.J., 2000. Iron and manganese in the Ross Sea, Antarctica: seasonal iron limitation in Antarctic shelf waters. J. Geophys. Res. 105, 11321. https://doi.org/10.1029/2000JC000256.
Serreze, M.C., Barry, R.G., 2011. Processes and impacts of Arctic amplification : a research synthesis. Global Planet. Change 77, 85–96. https://doi.org/10.1016/j.gloplacha.2011.03.004.
Shemesh, A., Burckle, L.H., Froelich, P.N., 1989. Dissolution and preservation of antarctic diatoms and the effect on sediment thanatocoenoses. Quat. Res. 31, 288–308.
Shimmield, G., Derrick, S., Mackensen, A., Grobe, H., Pudsey, C., 1994. The history of barium, biogenic silica and organic carbon accumulation in the Weddell Sea and Antarctic Ocean over the last 150,000 years. In: Zahn, R., Kaminski, M.A., Labeyrie, L., Pedersen, T.F. (Eds.), Carbon Cycling in the Glacial Ocean: Constraints on the Ocean's Role in Global Change, NATO ASI Series, vol. 117. Springer, Berlin, Heidelberg, New York, pp. 555–574.
Sigman, D.M., Fripiat, F., Studer, A.S., Kemeny, P.C., Martínez-García, A., Hain, M.P., Ai, X., Wang, X., Ren, H., Haug, G.H., 2021. The Southern Ocean during the ice ages: a review of the Antarctic surface isolation hypothesis, with comparison to the North Pacific. Quat. Sci. Rev. 254, 106732. https://doi.org/10.1016/j.quascirev.2020.106732.
Sigman, D.M., Hain, M.P., Haug, G.H., 2010. The polar ocean and glacial cycles in atmospheric CO2 concentration. Nature 466, 47–55. https://doi.org/10.1038/nature09149.
Sigman, D.M., Jaccard, S.L., Haug, G.H., 2004. Polar ocean stratification in a cold climate. Nature 428, 59–63. https://doi.org/10.1038/nature02378.1.
Sinninghe Damsté, J.S., 2016. Spatial heterogeneity of sources of branched tetraethers in shelf systems : the geochemistry of tetraethers in the Berau River delta (Kalimantan , Indonesia). Geochem. Cosmochim. Acta 186, 13–31. https://doi.org/10.1016/j.gca.2016.04.033.
Sinninghe Damsté, J.S., Ossebaar, J., Abbas, B., Schouten, S., Verschuren, D., 2009. Fluxes and distribution of tetraether lipids in an equatorial African lake : constraints on the application of the TEX 86 palaeothermometer and BIT index in lacustrine settings. Geochem. Cosmochim. Acta 73, 4232–4249. https://doi.org/10.1016/j.gca.2009.04.022.
Smith, J.A., Hillenbrand, C., Pudsey, C.J., Allen, C.S., Graham, A.G.C., 2010. The presence of polynyas in the Weddell Sea during the Last Glacial Period with implications for the reconstruction of sea-ice limits and ice sheet history. Earth Planet Sci. Lett. 296, 287–298. https://doi.org/10.1016/j.epsl.2010.05.008.
Smith Jr., W.O., Shields, A.R., Dreyer, J.C., Peloquin, J.A., Asper, V., 2011. Interannual variability in vertical export in the Ross Sea: magnitude, composition, and environmental correlates. Deep-Sea Res. Pt I 58, 147–159. https://doi.org/10.1016/j.dsr.2010.11.007.
Smith, W.O.J., Sedwick, P.N., Arrigo, K.R., Ainley, D.G., Orsi, A.H., 2012. The Ross Sea in a sea of change. Oceanography 25, 90–103.
Spreen, G., Kaleschke, L., Heygster, G., 2008. Sea ice remote sensing using AMSR-E 89-GHz channels. J. Geophys. Res. 113, C02S03. https://doi.org/10.1029/2005JC003384.
Steinacher, M., Joos, F., Frölicher, T.L., Bopp, L., Cadule, P., Cocco, V., Doney, S.C., Gehlen, M., Lindsay, K., Moore, J.K., Schneider, B., Segschneider, J., 2010. Projected 21st century decrease in marine productivity : a multi-model analysis. Biogeosciences 7, 979–1005.
Stephens, B.B., Keeling, R.F., 2000. The influence of Antarctic sea ice on glacial-interglacial CO2 variations. Nature 404, 171–174.
Stoecker, D.K., Gustafson, D.E., Baier, C.T., Black, M.M.D., 2000. Primary production in the upper sea ice. Aquat. Microb. Ecol. 21, 275–287. https://doi.org/10.3354/ame021275.
Strickland, J.D.H., Parsons, T.R., 1972. A Practical Handbook of Seawater Analysis, second ed. Fisheries Research Board of Canada, Ottawa.
Studer, A.S., Sigman, D.M., Martínez-García, A., Benz, V., Winckler, G., Kuhn, G., Esper, O., Lamy, F., Jaccard, S.L., Wacker, L., Oleynik, S., Gersonde, R., Haug, G.H., 2015. Antarctic Zone nutrient conditions during the last two glacial cycles. Paleoceanography 30. https://doi.org/10.1002/2014PA002745 n/a-n/a.
Tesi, T., Miserocchi, S., Goñi, M.A., Langone, L., 2007. Source , transport and fate of terrestrial organic carbon on the western Mediterranean Sea , Gulf of Lions. France. Mar. Chem. 105, 101–117. https://doi.org/10.1016/j.marchem.2007.01.005.
Thomas, E., Gooday, A.J., 1996. Cenozoic deep-sea benthic foraminifers: tracers for changes in oceanic productivity? Geology 24, 355–358. https://doi.org/10.1130/0091-7613(1996)024<0355:CDSBFT>2.3.CO.
Tierney, J.E., Tingley, M.P., 2014. A Bayesian, spatially-varying calibration model for the TEX86 proxy. Geochem. Cosmochim. Acta 127, 83–106. https://doi.org/10.1016/j.gca.2013.11.026.
Tierney, J.E., Tingley, M.P., 2015. A TEX_{86} surface sediment database and extende Bayesian calibration. Nature Sci. Dat. 2, 150029. https://doi.org/10.1038/sdata.2015.29.
Troedson, A.L., Riding, J.B., 2002. Upper oligocene to lowermost miocene strata of king George Island, south Shetland Islands, Antarctica: stratigraphy, facies analysis, and implications for the glacial history of the antarctic peninsula. J. Sediment. Res. 72, 510–523. https://doi.org/10.1306/110601720510.
Turner, J., Comiso, J.C., Marshall, G.J., Lachlan-cope, T.A., Bracegirdle, T., Maksym, T., Meredith, M.P., Wang, Z., Orr, A., 2009. Non-annular Atmospheric Circulation Change Induced by Stratospheric Ozone Depletion and its Role in the Recent Increase of Antarctic Sea Ice Extent 36, 1–5. https://doi.org/10.1029/2009GL037524.
Turner, J., Phillips, T., Marshall, G.J., Hosking, J.S., Pope, J.O., Bracegirdle, T.J., Deb, P., 2017. Unprecedented springtime retreat of Antarctic sea ice in 2016. Geophys. Res. Lett. 44, 6868–6875. https://doi.org/10.1002/2017GL073656.
Vancoppenolle, M., Bopp, L., Madec, G., Dunne, J., Ilyina, T., Halloran, P.R., Steiner, N., 2013. Future Arctic Ocean primary productivity from CMIP5 simulations : uncertain outcome , but consistent mechanisms. Global Biogeochem. Cycles 27, 605–619. https://doi.org/10.1002/gbc.20055.
Veres, D., Bazin, L., Landais, A., Toyé Mahamadou Kele, H., Lemieux-Dudon, B., Parrenin, F., Martinerie, P., Blayo, E., Blunier, T., Capron, E., Chappellaz, J., Rasmussen, S.O., Severi, M., Svensson, A., Vinther, B., Wolff, E.W., 2013. The Antarctic ice core chronology (AICC2012): an optimized multi-proxy and multi-site dating approach for the last 120 thousand years. Clim. Past 9, 1733–1748.
Versteegh, G.J.M., Zonneveld, K.A.F., 2002. Use of selective degradation to separate preservation from productivity, pp. 615–618.
Warny, S., Kymes, C.M., Askin, R.A., Krajewski, K.P., Bart, P.J., 2016. Remnants of antarctic vegetation on king George Island during the early miocene melville glaciation. Palynology 40, 66–82. https://doi.org/10.1080/01916122.2014.999954.
Warny, S., Wrenn, J.H., Bart, P.J., Askin, R., 2006. Palynology of the NBP03-01 A transect in the northern basin, western Ross Sea, Antarctica: a late Pliocene record. Palynology 30, 151–182.
Weijers, J.W.H., Lim, K.L.H., Aquilina, A., Sinninghe Damsté, J.S., Pancost, R.D., 2011. Biogeochemical controls on glycerol dialkyl glycerol tetraether lipid distributions in sediments characterized by diffusive methane flux. Geochem. Geophys. Geosy. 12, Q10010. https://doi.org/10.1029/2011GC003724.
Weijers, J.W.H., Schefuß, E., Kim, J., Sinninghe, J.S., Schouten, S., 2014. Constraints on the sources of branched tetraether membrane lipids in distal marine sediments. Org. Geochem. 72, 14–22. https://doi.org/10.1016/j.orggeochem.2014.04.011.
Wilson, D.J., Bertram, R.A., Needham, E.F., Flierdt, T., Van, De, Welsh, K.J., Mckay, R.M., Mazumder, A., Riesselman, C.R., Jimenez-espejo, F.J., Escutia, C., 2018. Ice loss from the East antarctic ice sheet during late Pleistocene interglacials. Nature. https://doi.org/10.1038/s41586-018-0501-8.
Wilson, G.S., Roberts, A.P., Verosub, K.L., Florindo, F., Sagnotti, L., 1998. Magnetobiostratigraphic chronology of the Eocene-Oligocene transition in the CIROS-1 core, Victoria Land margin, Antarctica: implications for Antarctic glacial history. Bull. Geol. Soc. Am. 110, 35–47. https://doi.org/10.1130/0016-7606(1998)110<0035:MCOTEO>2.3.CO, 2.
Wrenn, J.H., Hannah, M.J., Raine, J.I., 1998. Diversity and Palaeoenvironmental significance of late cainozoic marine palynomorphs from the CRP-1 core, Ross Sea, Antarctica. Terra Antartica 5, 553–570.
Xiao, W., Frederichs, T., Gersonde, R., Kuhn, G., Esper, O., Zhang, X., 2016. Quaternary geochronology constraining the dating of late quaternary marine sediment records from the Scotia sea (Southern Ocean). Quat. Geochronol. 31, 97–118. https://doi.org/10.1016/j.quageo.2015.11.003.
Yamamoto, M., Shimamoto, A., Fukuhara, T., Tanaka, Y., Ishizaka, J., 2012. Glycerol dialkyl glycerol tetraethers and TEX86 index in sinking particles in the western North Pacific. Org. Geochem. 53, 52–62. https://doi.org/10.1016/j.orggeochem.2012.04.010.
Zell, C., Kim, J., Hollander, D., Lorenzoni, L., Baker, P., Guizan, C., Nittrouer, C., 2014. Sources and distributions of branched and isoprenoid tetraether lipids on the Amazon shelf and fan : implications for the use of GDGT-based proxies in marine sediments. Geochem. Cosmochim. Acta 139, 293–312. https://doi.org/10.1016/j.gca.2014.04.038.

Zhang, J., 2007. Increasing antarctic sea ice under warming atmospheric and oceanic conditions. J. Clim. 20, 2515–2529. https://doi.org/10.1175/JCLI4136.1.
Zhang, Y.G., Pagani, M., Wang, Z., 2016. Ring Index: a new strategy to evaluate the integrity of TEX86 paleothermometry. Paleoceanography 31, 220–232. https://doi.org/10.1002/2015PA002848.Received.
Zhang, Y.G., Zhang, C.L., Liu, X., Li, L., Hinrichs, K., Noakes, J.E., 2011. Methane Index : a tetraether archaeal lipid biomarker indicator for detecting the instability of marine gas hydrates. https://doi.org/10.1016/j.epsl.2011.05.031, 307, 525, 534.
Zielinski, U., Gersonde, R., 2002. Plio-pleistocene diatom biostratigraphy from ODP leg 177, Atlantic sector of the Southern Ocean. Mar. Micropaleontol. 45, 225–268. https://doi.org/10.1016/S0377-8398(02)00031-2.
Zielinski, U., Gersonde, R., 1997. Diatom distribution in Southern Ocean surface sediments (Atlantic sector): implications for paleoenvironmental reconstructions. Palaeogeogr. Palaeocl. 129, 213–250. https://doi.org/10.1016/S0031-0182(96)00130-7.
Zonneveld, K.A.F., Versteegh, G.J., Kasten, S., Eglinton, T.I., Emeis, K.C., Huguet, C., Koch, B.P., De Lange, G.J., De Leeuw, J.W., Middelburg, J.J., Mollenhauer, G., Prahl, F.G., Rethemeyer, J., Wakeham, S.G., 2010. Selective preservation of organic matter in marine environments; processes and impact on the sedimentary record. Biogeosciences 7, 483–511.
Zonneveld, K.A.F., Marret, F., Versteegh, G.J.M., Bogus, K., Bonnet, S., Bouimetarhan, I., Crouch, E., De Vernal, A., Elshanawany, R., Edwards, L., Esper, O., Forke, S., Grøsfjeld, K., Henry, M., Holzwarth, U., Kielt, J., Kim, S., Ladouceur, S., Ledu, D., Chen, L., Limoges, A., Londeix, L., Lu, S.-H., Mahmoud, M.S., Marino, G., Matsouka, K., Matthiessen, J., Mildenhal, D.C., Mudie, P., Neil, H.L., Pospelova, V., Qi, Y., Richerol, T., Rochon, A., Sangiorgi, F., Solignac, S., Turon, J., Verleye, T., Wang, Y., Wang, Z., Young, M., 2013. Atlas of modern dinoflagellate cyst distribution based on 2405 data points. Rev. Palaeobot. Palynol. 191, 1–197. https://doi.org/10.1016/j.revpalbo.2012.08.003.